Uncovering Phenotypic Expansion in AXIN2-Related Disorders through Precision Animal Modeling

Nathalie M. Aceves-Ewing[1,*], Denise G. Lanza[1,*], Paul C. Marcogliese[2,3,*], Di Lu[1,4], Chih-Wei Hsu[5,6], Matthew Gonzalez[1], Audrey E. Christiansen[5], Tara L. Rasmussen[5], Alex J. Ho[7,8], Angelina Gaspero[1], John Seavitt[1], Mary E. Dickinson[1,5], Bo Yuan[1,9], Brian J. Shayota[10], Stephanie Pachter[11], Xiaolin Hu[12], Debra Lynn Day-Salvatore[13], Laura Mackay[14], Oguz Kanca[1,4], Michael F. Wangler[1,5], Lorraine Potocki[1,15], Jill A. Rosenfeld[1], Richard Alan Lewis[1], Hsiao-Tuan Chao[1,4,15,16,17,18,19], Brendan Lee[1,15], Sukyeong Lee[7,8], Undiagnosed Diseases Network[20], Baylor College of Medicine Center for Precision Medicine Models[21], Shinya Yamamoto[1,4,16] , Hugo J. Bellen[1,4,16,*], Lindsay C. Burrage[1,15,*, #], Jason D. Heaney[1,22,*, #]

[1] Department of Molecular and Human Genetics, Baylor College of Medicine (BCM), Houston, TX, 77030, USA
[2] Department of Biochemistry and Medical Genetics, Rady Faculty of Health Sciences, University of Manitoba, Winnipeg, MB, R3E 0J9, Canada
[3] Children's Hospital Research Institute of Manitoba (CHRIM), Winnipeg, MB, R3E 3P4, Canada
[4] Jan and Dan Duncan Neurological Research Institute, Texas Children's Hospital (TCH), Houston, TX, 77030, USA
[5] Department of Integrative Physiology, Baylor College of Medicine, Houston, TX, 77030, USA
[6] Optical Imaging and Vital Microscopy Core, Baylor College of Medicine, Houston, TX, 77030, USA
[7] Verna and Marrs McLean Department of Biochemistry and Molecular Pharmacology, Baylor College of Medicine, Houston, TX, 77030, USA
[8] Advanced Technology Core for Macromolecular X-ray Crystallography, Baylor College of Medicine, Houston, TX, 77030, USA
[9] Human Genome Sequencing Center, Baylor College of Medicine, Houston, TX, 77030, USA
[10] Division of Medical Genetics, Department of Pediatrics, University of Utah, Salt Lake City, UT, 84108, USA
[11] Atlantic Health System, Summit, NJ 07901, USA
[12] GeneDX, Gaithersburg MD, 20877, USA
[13] Department of Medical Genetics and Genomic Medicine, Saint Peter's University Hospital, New Brunswick, NJ, 08901, USA
[14] Department of Pediatrics, Division of Genetics and Metabolism, University of Texas Southwestern Medical Center, Dallas, TX, USA
[15] Texas Children's Hospital, Houston, TX, 77030, USA
[16] Department of Neuroscience, BCM, Houston, TX, 77030, USA
[17] The Cain Pediatric Neurology Research Foundation Laboratories, Jan and Dan Duncan Neurological Research Institute, Texas Children's Hospital, Houston, Texas, USA
[18] McNair Medical Institute, The Robert and Janice McNair Foundation, Houston, Texas, USA
[19] Division of Neurology and Developmental Neuroscience, Department of Pediatrics, Baylor College of Medicine, Houston, Texas, USA
[20] Member list in supplemental material
[21] Member list in supplemental material
[22] Dan L. Duncan Comprehensive Cancer Center, Baylor College of Medicine, Houston, TX, 77030, USA
* These authors contributed equally
# Co-corresponding; emails: burrage@bcm.edu; heaney@bcm.edu

Keywords: ectodermal dysplasia, WNT/β-catenin signaling, oligodontia-colorectal cancer, AXIN2, tankyrase-binding domain

Abstract

Heterozygous pathogenic variants in *AXIN2* are associated with oligodontia-colorectal cancer syndrome (ODCRCS), a disorder characterized by oligodontia, colorectal cancer, and in some cases, sparse hair and eyebrows. We have identified four individuals with one of two *de novo*, heterozygous variants (NM_004655.4:c.196G>A, p.(Glu66Lys) and c.199G>T, p.(Gly67Arg)) in *AXIN2* whose presentations expand the phenotype of AXIN2-related disorders. In addition to ODCRCS features, these individuals have global developmental delay, microcephaly, and limb, ophthalmologic, and renal abnormalities. Structural modeling of these variants suggests that they disrupt AXIN2 binding to tankyrase, which regulates AXIN2 levels through PARsylation and subsequent proteasomal degradation. To test whether these variants produce a phenotype *in vivo*, we utilized an innovative prime editing N1 screen to phenotype heterozygous (p.E66K) mouse embryos, which were perinatal lethal with short palate and skeletal abnormalities, contrary to published viable *Axin2* null mouse models. Modeling of the p.E66K variant in the *Drosophila* wing revealed gain-of-function activity compared to reference AXIN2. However, the variant showed loss-of-function activity in the fly eye compared to reference AXIN2, suggesting that the mechanism by which p.E66K affects AXIN2 function is cell context-dependent. Together, our studies in humans, mice, and flies demonstrate that specific variants in the tankyrase-binding domain of AXIN2 are pathogenic, leading to phenotypic expansion with context-dependent effects on AXIN2 function and WNT signaling. Moreover, the modeling strategies used to demonstrate variant pathogenicity may be beneficial for the resolution of other *de novo* heterozygous variants of uncertain significance associated with congenital anomalies in humans.

Introduction

The canonical WNT signaling pathway, also referred to as the β-catenin-dependent WNT pathway, is evolutionarily conserved and critical to embryonic development and adult homeostasis in nearly all animals. Since the WNT/β-catenin pathway is involved in many early developmental processes and in the maintenance of cell proliferation, diseases associated with dysregulated WNT signaling include a wide range of Mendelian and non-Mendelian phenotypes and several types of cancer. Some of the known disorders associated with aberrant WNT signaling include tooth agenesis[1-4], neurodegenerative disorders[5-7], and renal disease[8]. Cancers associated with members of the WNT signaling pathway include breast cancer[9-11], hepatocellular carcinoma[11-13], and colorectal cancer[1-3,11,13-17].

The inhibition and activation of the canonical WNT/β-catenin pathway involves multiple extracellular, membrane-bound, cytoplasmic, and nuclear proteins[18-22]. In the absence of WNT ligand binding to the receptor complex consisting of FZD and LRP5/6, β-catenin is constitutively phosphorylated by the destruction complex (composed of APC, CK1, GSK3β, and AXIN1 or AXIN2), leading to its ubiquitination and proteasomal degradation[21,23-28]. However, upon WNT binding, the activity of the destruction complex is inhibited and accumulated β-catenin translocates to the nucleus, where it associates with TCF/LEF transcription factors to activate the expression of genes involved in cell fate determination, cell proliferation, and other key cellular processes[14,26,27]. Critically, in some cell contexts AXIN2 can also positively regulate WNT signaling by binding to and maintaining the phosphorylation of the LRP5/6 receptors after WNT activation of its receptor complex[29-32].

Somatic variants in *AXIN2* have been associated with somatic colorectal cancer (MIM #114500) whereas germline variants in *AXIN2* have been associated with oligodontia-colorectal cancer syndrome (ODCRCS, MIM #608615)[1-4,9,10,15,16,33]. ODCRCS most commonly includes phenotypes such as oligodontia, colon polyps, colorectal cancer, and sparse hair and eyebrows[1-4,9,10,15,16,33,34]. To date, most published pathogenic variants in *AXIN2* cluster towards the C-terminus of the protein as well as a few variants in the Regulator of G protein signaling (RGS), GSK3β-binding, and β-catenin-binding domains[1-4,9,15,16]. However, to date, no pathogenic variants have been identified in the tankyrase (TNKS)-binding domain[1-4,15,16,35-37]. This domain is necessary for TNKS binding, which leads to the poly-ADP-ribosylatation (PARsylation), ubiquitination, and proteasomal degradation of AXIN2[35,37].

In this study, we report three individuals with ectodermal dysplasia, musculoskeletal anomalies, genitourinary abnormalities, and a *de novo* heterozygous variant in the TNKS-binding domain (p.Glu66Lys, referred to as E66K) of AXIN2. As pathogenic variants in this domain have not been previously reported and as the phenotype associated with these variants was hypothesized to be lethal in mice, we combined structural and fly modeling with innovative mouse modeling strategies to demonstrate the pathogenicity of the p.E66K variant. In addition, we used amino acid conservation and population databases to identify a neighboring variant (p.Gly67Arg, referred to as G67R) that causes an overlapping human phenotype. Overall, we demonstrate that variants impacting key residues in the TNKS-binding domain of AXIN2 represent a phenotypic expansion and novel ectodermal dysplasia associated with congenital anomalies.

Materials and Methods

Clinical Study. Participant 1 and both parents were enrolled in the Baylor College of Medicine (BCM) site for the Undiagnosed Diseases Network (UDN). This study was approved by the Institutional Review Board (IRB) at both the National Institutes of Health and BCM. The family provided written informed consent prior to the initiation of any research procedures. Additional cases (participants 2, 3, and 4) were identified through a search of ClinVar[38] for variants at the same or nearby positions and communications with the submitters of these variants (GeneDx and Invitae). Participants 2, 3, and 4 and their families also provided written informed consent prior to the initiation of research procedures under an IRB-approved protocol at BCM. *As per medRxiv policy, the case histories for the participants and their images have been removed. To obtain more detailed information, please contact the authors.*

Exome and Genome Sequencing. For participant 1, clinical trio exome sequencing was performed at Baylor Genetics as previously described[39] and transferred to the BCM UDN site for research re-analysis. Trio genome sequencing was performed through the UDN Sequencing Core at Baylor Genetics as previously described[40], and research reanalysis was performed at the BCM UDN site. The research exome and genome re-analyses prioritized rare, *de novo* and biallelic variants that had an allele frequency of < 1% in gnomAD v4.0.0[41] and in the BCM UDN internal sequencing database (> 1200 samples). Codified Genomics was used for variant filtering and prioritization. Participant 2's variant was detected on an Invitae Hereditary Colorectal Cancer panel as part of an evaluation for colon polyps. This next generation sequencing panel included 20 genes associated with predisposition to colorectal cancer. Sanger sequencing was performed using DNA extracted from parental buccal samples at Baylor Genetics Laboratory to confirm that the *AXIN2* variant identified in participant 2 is *de novo*.

Participants 3 and 4 had clinical trio exome sequencing performed through GeneDx. For CADD Scores, CADD GRCh37-v1.7 was used.

Conservation alignments. The conservation alignments were made using default parameters in Clustal Omega (CLUSTAL O(1.2.4) multiple sequence alignment)[42-44] with *Homo sapiens* AXIN2 (Q9Y2T1) as the reference sequence aligned with *Mus musculus* AXIN2 (O88566), and *Homo sapiens* (O15169) and *Mus musculus* (O35625) AXIN1. Amino acid sequences were acquired from UniProt[45]. A similar alignment was performed using *Homo sapiens* AXIN2 (Q9Y2T1) as the reference sequence aligned with fly (*Drosophila melanogaster*) AXN (Q9V407) and AXIN2 amino acid sequences from the following organisms: *Mus musculus* (O88566), *Rattus norvegicus* (O70240), *Pan troglodytes* (K7CHS6), *Gorilla gorilla gorilla* (G3QN00), *Macaca mulatta* (A0A5F8AE66), *Pongo abelii* (H2NUH3), *Papio anubis* (A0A096NTX5), *Chlorocebus sabaeus* (A0A0D9QVR2), *Otolemur garnettii* (H0WYQ7), *Microcebus murinus* (A0A8B7F524), *Ictidomys tridecemlineatus* (I3N719), *Canis lupus familiaris* (A0A8C0YRK8), *Felis catus* (M3XAL0), *Mustela putorius furo* (M3YT87), *Ailuropoda melanoleuca* (G1LZK8), *Equus caballus* (F6SK96), *Pteropus vampyrus* (A0A6P6CVR3), *Bos taurus* (G3X7P3), *Sus scrofa* (A0A287BFQ6), *Tursiops truncates* (A0A6J3QL77), *Sarcophilus harrisii* (G3VT89), *Monodelphis domestica* (F6TVK6), *Anolis carolinensis* (H9G5B4), *Pelodiscus sinensis* (K7G9P5), *Gallus gallus* (A0A1D5PPH8), *Latimeria chalumnae* (H3BCV4), *Ficedula albicollis* (U3JIC1), *Danio rerio* (P57095), *Oreochromis niloticus* (I3J624), *Xiphophorus maculatus* (A0A3B5QRG9), *Oryzias latipes* (H2L981), *Tetraodon nigroviridis* (H3C937), *Gasterosteus aculeatus* (G3Q3K5), *Xenopus tropicalis* (A0A803JRP4), *Astyanax mexicanus* (A0A3B1KDC5), and *Takifugu rubripes* (H2SP31).

174 **Structural modeling.** The side chains of the mutated E66K and G67R residues in the TNKS
175 binding motif 2 (TBM2) of AXIN2 were modeled based on the crystal structure of the TNKS
176 ankyrin-repeat clusters 2-3 (ARC2-3) and AXIN1 complex (PDB ID: 3UTM) as a template[37]. For
177 each variant, a rotamer conformation was selected for the mutated residue to model the side
178 chain, followed by minor adjustments of the *chi* angles. Structural modelling was performed using
179 Coot[46].
180

181 **Mouse colony management.** All mice were housed in microisolator cages in ventilated racks
182 within the ABBR animal facility at BCM. The rooms were temperature controlled and humidity
183 controlled with a 6:00 AM to 8:00 PM light:dark cycle. The mice were given *ad libitum* access to
184 food (Lab Diet 5V5R) and autoclaved drinking water for the duration of the study. All studies
185 were approved by the BCM Institutional Animal Care and Use Committee.

186

187 ***Axin2* p.E66K founder embryo screen.** To generate founder embryos harboring a knock-in
188 (KI) of the p.E66K (GAG>AAG) point mutation, as well as a p.G67 (GGG>GGC) synonymous
189 mutation, two different design strategies were implemented, each using a single guide RNA
190 (sgRNA) with a complementary single-stranded oligodeoxynucleotide (ssODN) repair donor for
191 CRISPR/Cas9-initiated homology-directed repair (**Figure S1**). Inclusion of the synonymous
192 mutation in the ssODN sequence alters the sgRNA target sequence, thus reducing guide affinity
193 and suppressing secondary CRISPR genome editing events after homology-directed repair. The
194 sgRNAs were selected by the BCM Genetically Engineered Rodent Model (BCM GERM) Core
195 using the Wellcome Sanger Institute Genome Editing (WGE) website[47]. Complementary to the
196 strand of the target site, corresponding ssODNs were designed with asymmetric homology arms
197 flanking the p.E66K mutation relative to the predicted cut site of the gRNA. Sequences and
198 genomic coordinates can be found in **Table S1**. The sgRNAs were synthesized by Synthego

199 and custom ssODNs (Ultramers) were produced by Integrated DNA Technologies (Coralville,
200 IA). The BCM GERM Core electroporated a mixture consisting of precomplexed sgRNA (6.6
201 μM) and Cas9 Protein (6 μM, PNA Bio), ssDNA mRNA (100 pmol) in a final volume of 10 μL
202 1xTE (RNAse-free) into at least 60 pronuclear stage C57BL/6J (Jackson Lab Strain #:000664;
203 RRID:IMSR_JAX:000664) zygotes as previously described[48]. Embryos were transferred to
204 pseudopregnant females the same day as electroporation and allowed to gestate for 18 days
205 prior to sacrifice of the recipient dam and collection of embryos for subsequent genotyping and
206 imaging.

207

208 ***Axin2$^{E66K/+}$* constitutive knock-in mouse model.** To generate a constitutive knock-in (KI)
209 mouse model with the p.E66K (GAG>AAG) point mutation as well as a p.G67 (GGA>GGG)
210 synonymous mutation, RNA-guided nuclease prime editing was utilized (**Figure S2A)**. A prime
211 editing guide RNA (pegRNA) and a complementary sgRNA to facilitate DNA nicking were
212 selected by the BCM GERM Core using Peg Finder[49]. Again, the synonymous mutation was
213 included to suppress secondary genome editing events. Target sequences, genomic
214 coordinates, and guide sequences can be found in **Table S2 and S3**. The pegRNA was
215 purchased as a custom gRNA from Integrated DNA Technologies (Coralville, IA) and the nicking
216 gRNAs as synthesized sgRNAs from Synthego (Redwood City, CA). Prime editor (PE2) mRNA
217 was generated from linearized plasmid DNA (pCMV-PE2, addgene.org/132775/) using the
218 mMESSAGE mMACHINE T7 ULTRA Transcription Kit (ThermoFisher, AM1345). The BCM
219 GERM Core microinjected a mixture consisting of pegRNA (75ng/μL), sgRNA (75ng/μL), and
220 PE2 mRNA (150ng/μL) in a final volume of 50 μL 1xTE (RNAse-free) into the cytoplasm of
221 C57BL/6J (Jackson Lab Strain #:000664; RRID:IMSR_JAX:000664) pronuclear stage zygotes
222 as previously described[50]. DNA was isolated from ear punches and PCR was performed with
223 AmpliTaq Gold 360 Master Mix (Applied Biosystems, 4398881) using primers Axin2 E2 F (5'

224 TCCAGAGAGGAGGCTCACAT) and Axin2 E2 R (5' AAACATGACCGAGCCGATCT). PCR
225 products were Sanger sequenced and Synthego ICE analysis identified a founder male with
226 approximately 20% mosaicism for an allele harboring the p.E66K point mutation and p.G67
227 synonymous mutation, as well as a p.S70 (TCG>TCC) synonymous mutation (**Figure S2B)**.
228 This founder was used for breeding and subsequently sperm cryopreservation using the CARD
229 method[51,52]. The allele is registered at Mouse Genome Informatics (MGI) as *Axin2*^{em1Bay}
230 (MGI:7768058).

231

232 **Embryo phenotyping.** For the p.E66K embryo founder screen, embryos were collected at
233 embryonic day (E)18.5, fixed in 4% paraformaldehyde (PFA), and stored at 4°C until they could
234 be processed for µCT imaging, as previously described[53]. To generate N1 embryos harboring a
235 *Axin2*$^{E66K/+}$ constitutive knock-in allele, timed matings between the *Axin2*$^{E66K/+}$ mosaic male
236 founder and wild-type C57BL/6J females or *in vitro* fertilization with mosaic male sperm and
237 wild-type C57BL/6J oocytes were used as previously described[52,54,55]. Timed matings were set
238 up between male and female mice during the afternoon. If a vaginal plug was confirmed the
239 next morning, female and male mice were separated, and embryos were stated to be at E0.5.
240 Embryos were analyzed upon dissection at E18.5 with light microscopy. For µCT imaging, E18.5
241 embryos were fixed and processed as described for the founder screen. Embryos were scanned
242 with a Bruker SkyScan 1272 µCT Scanner, and images were analyzed with Slicer (v5.2.2).
243 Annotation of phenotypes was performed blinded to genotypes.

244

245 **Embryo genotyping.** DNA was extracted from yolk sacs for PCR-based genotyping and
246 Sanger sequencing. PCR was performed with AmpliTaq Gold 360 Master Mix using primers
247 Axin2 E2 F (5' TCCAGAGAGGAGGCTCACAT) and Axin2 E2 R (5'

248 AAACATGACCGAGCCGATCT). For the founder embryo screen, PCR products were Sanger
249 sequenced, and Synthego Inference of CRISPR Edits (ICE) analysis was used to determine
250 wild-type, insertion/deletion (non-homologous end joining), and variant (homology-directed
251 repair) allele contribution in each embryo. For N1 embryos derived from the mosaic *Axin2*$^{E66K/+}$
252 constitutive knock-in founder male, the same primers were used to generate PCR products,
253 which were subsequently digested with StyI High-Fidelity enzyme (NEB, R3500S). The
254 expected size for the wild-type product is 653 bp; StyI cleaves at the p.E66K sequence in the
255 *Axin2*^{E66K} allele, resulting in 335 bp and 318 bp products (**Figure S2A&C**). Transmission of the
256 *Axin2*$^{E66K/+}$ constitutive knock-in allele from the mosaic founder to N1 embryos was also
257 confirmed via Sanger sequencing (**Figure S2B**).

258

259 **Generation of AXIN2 transgenic flies.** *UAS-AXIN2* reference and variant transgenic flies were
260 generated as previously described[56]. Specifically, the Gateway compatible *AXIN2*
261 (NM_004655.4) open-reading frame (ORF) in the DONR221 vector was shuttled to the pGW-
262 HA.attb[57] UAS destination vector by LR clonase II (Invitrogen) by manufacturer protocol. The
263 ORF harbors an endogenous stop codon, thus this closed clone will not be tagged with HA.
264 Variants were generated via site-directed mutagenesis with the Q5 mutagenesis kit (NEB)
265 followed by verification of the ORF by Sanger sequencing. Primers used for site-directed
266 mutagenesis for the *AXIN2* p.E66K, R656X, and W663X variants are listed in **Table S4**. Final
267 UAS constructs were microinjected into embryos containing the VK37 (PBac{y[+]-
268 attP}VK00037) genomic docking site and integrated by ϕC31 mediated transgenesis[58].

269

270 **Generation of *AxnTG4* mutant flies.** The *Axn*^{TG4} (*Axn*$^{CR70218\text{-}TG4.2}$; BL_ 93803 – BDSC) allele
271 was generated in a previous study as part of the large-scale gene disruption project[59]. Briefly,

272 we generated homology donor intermediates to target an intron separating two exons in the
273 coding region of *Axn*. Construct with homology arms (200 bases upstream and downstream of
274 the target site) and *Axn*-specific sgRNA that targets the site
275 (TCATCGAGTCAGTGGTGTAGAGG) was commercially synthesized in pUC57_Kan_gw_OK2
276 vector by Genewiz/Azenta. The sequence comprising a cassette that includes attP-FRT-splice
277 acceptor-T2A-GAL4-poly(A)-3×P3EGFP-poly(A)-FRT-attP was transferred from the pM37 vector
278 to the intermediary vector designed for homology, thereby generating a new homology donor
279 vector. The construct was injected at 250 ng/µl final concentration into 664 embryos from the
280 line: *y^1w^*; attP40(y+){nos-Cas9(v+)}; iso50.* Eclosed flies were crossed with *y^1 w** flies, and the
281 3×P3–EGFP-positive progeny were selected based on GFP expression in the adult eyes.

282

283 **Protein Quantification.** To determine human AXIN2 protein level upon overexpression in flies,
284 *AXIN2* reference and variants were expressed pan-neuronally with *elav-GAL4*. Five fly heads
285 from each genotype were homogenized in a cell lysis buffer (RIPA buffer, 1X liquid protease
286 inhibitor (Gen DEPOT)) with an electric Dounce on ice. Next, Laemmli buffer and 5% β-
287 mercaptoethanol (BME) was added to each tube and lysed heads were incubated on ice for 10
288 minutes and boiled for five minutes at 95°C. Samples were centrifuged at 14,000 RPM for five
289 minutes at 4°C. The supernatant was loaded into 4-20% gradient gels (Mini-PROTEAN®
290 TGX™), separated by SDS-PAGE, and transferred to nitrocellulose membranes (Bio-Rad). The
291 following primary antibodies were used in this study: anti-Actin (mouse monoclonal: C4;
292 1:20,000) (EMD Millipore), anti-AXIN2 (rabbit monoclonal: 76G6; #2151; 1:1000) (Cell
293 Signaling). Corresponding HRP-conjugated secondaries were used at 1:10,000 dilution.

294

295 **Immunostaining and imaging.** The methods for preparing and visualizing *Drosophila* wing
296 discs were performed as previously reported[60]. To summarize, wing discs from third-instar
297 larvae at the wandering stage were dissected and preserved in 4% PFA. These samples were
298 subsequently immunostained with the following antibodies: mouse anti-Wingless at a dilution of
299 1:50 (Developmental Studies Hybridoma Bank [DSHB], clone 4D4), mouse anti-Cut at the same
300 dilution (DSHB, clone 2B10), and guinea pig anti-Senseless at a dilution of 1:100[61]. For the
301 mounting phase, Vectashield (Vector Labs, H-1000-10) was employed. The wing discs were
302 examined using a Zeiss LSM 880 laser confocal microscope. For the post-scanning image
303 enhancement, ZEN software from Zeiss and Imaris software from Oxford Instruments were
304 utilized.

305

306 **Adult wing and eye preparation and imaging.** Adult *Drosophila* wings were dissected and
307 mounted as previously described[60]. Briefly, wings from adult flies were excised and preserved in
308 70% ethanol before being arranged in a solution made from a mixture of CMCP-10 mounting
309 medium (sourced from Masters in Wood Dale, IL) and lactic acid in a ratio of 3 to 1. For eyes,
310 whole flies of appropriate genotypes were frozen at -20ºC for 24 hours before imaging. The
311 images for adult wings and eyes were captured using a Leica MZ16 stereomicroscope that was
312 outfitted with an Optronics MicroFire camera and operated using Image-Pro Plus software
313 version 7.0.

314

315 **Statistical Analyses.** A two-sided Fisher's exact test to determine if there was a significant
316 difference between genotype distribution across E18.5 and postnatal timepoints for the
317 *Axin2*$^{E66K/+}$ embryos and *Axin2*$^{+/+}$ littermates was done using GraphPad Prism (version 10.3.1

318 (509)). For *Drosophila* studies and quantification, ANOVA was followed by Tukey's post hoc test
319 using GraphPad Prism.

320

321 **Results**

322 ***De novo* heterozygous variants clustered in the TNKS-binding domain of AXIN2 cause**
323 **multiple congenital anomalies.** A cohort consisting of three individuals with the same
324 heterozygous *de novo* variant in *AXIN2* (NM_004655.4:c.196G>A, p.E66K) and overlapping
325 phenotype consisting of features of an ectodermal dysplasia as well as skeletal and
326 genitourinary anomalies was identified through the UDN and ClinVar. This variant was not
327 present in gnomAD(v4.0.0)[41] or in the BCM clinical site internal sequencing database. The
328 CADD score is 27.2[62], Revel score is 0.549[63], and AlphaMissense score is 0.765[64]. The glutamic
329 acid at this position is in the TNKS-binding domain of AXIN2[65] and is conserved in vertebrates
330 including mice and in zebrafish but not in *Drosophila melanogaster* (**Figure 1A and Figure**
331 **S3A**). This variant has been reported in the Catalogue of Somatic Mutations in Cancer
332 (COSMIC, v100) one time in a large intestinal adenocarcinoma from a 64-year-old male[66].

333

334 Based on structural modeling data of AXIN1 and tankyrase interactions[37], the proline at position
335 65 and the glycine at position 67 in AXIN2 are critical for the interaction between AXIN2 and
336 tankyrase[37]. Given that there is an absence of missense variation at these positions in
337 gnomAD(v4.0.0) (**Figure 1B, Figure S3B**) in conjunction with the conservation data, we
338 hypothesized that variants impacting positions 65 and 67 might cause phenotypes similar to
339 those with variants at position 66. Thus, we searched ClinVar for missense variation impacting
340 these neighboring amino acids. This search identified participant 4 with a similar phenotype who
341 has a *de novo* heterozygous variant at position 67 (NM_004655.4:c.199G>A, p.G67R). The

342 CADD score of the p.G67R variant is 27.4, REVEL score is 0.494, and AlphaMissense score is
343 0.971. This glycine is conserved in vertebrates including mice and zebrafish but not in
344 *Drosophila melanogaster*. This variant was also observed as a confirmed somatic heterozygous
345 variant in a large intestinal adenocarcinoma sample from a female of unknown age and a diffuse
346 adenocarcinoma of the stomach from a 38-year-old female in the COSMIC database(v100).

347

348 The phenotype observed in the four individuals with *de novo* heterozygous variants impacting
349 the glutamic acid at position 66 or the glycine at position 67 of AXIN2 is complex and variable.
350 Common phenotypes include digit and limb anomalies (4/4), global developmental delay (3/4),
351 microcephaly (3/4), ophthalmologic complications (3/4), genitourinary anomalies (3/4), unique
352 facial features (3/4), and palate abnormalities (2/4). Features suggestive of an ectodermal
353 dysplasia such as oligodontia (3/4), sparse hair (3/4), sparse eyebrows and eyelashes (3/4),
354 and nail abnormalities (2/4) are common. These findings together with sagittal craniosynostosis
355 suggested a diagnosis of cranioectodermal dysplasia in participant 3. Although three of the four
356 patients are children with complex phenotypes identified by exome or genome sequencing, one
357 individual is an adult whose variant in *AXIN2* was identified on a colorectal cancer panel. This
358 adult has a milder, but overlapping phenotype which includes digit abnormalities, skeletal
359 abnormalities, and history of vesicoureteral reflux in addition to a diagnosis of colon cancer with
360 >25 colon polyps. Detailed case reports are provided in supplemental material.

361

362 **Structural modeling.** Since no atomic structure is available for the TNKS/AXIN2 complex, we
363 attempted structure prediction of this complex *in silico* using AlphaFold2-multimer[67] initially, and
364 later using AlphaFold3[68]. TNKS proteins contain an ankyrin-repeat domain that consists of a
365 series of ankyrin-repeat clusters (ARCs)[37]. In the top five prediction results from AlphaFold2-

366 multimer, the first TNKS binding motif (TBM1) in AXIN2 binds the ankyrin-repeat domain ARC4 in
367 all five predicted structures, while the second binding motif (TBM2) binds to ARC5 in one predicted
368 structure. However, all five top predictions from AlphaFold3 shows only TBM2 binding to ARC5.
369 Pairwise comparison of the Alphafold predicted structure and the known crystal structure of the
370 ARC domain of TNKS with bound peptide (PDB IDs: 3UTM and 3TWW) shows that the peptide
371 binding interactions are very similar, with the peptides interacting on the same surface of ARC.
372 Currently, it is unclear which ARC of TNKS is the binding partner for each TBM. However, based
373 on results from the pulldown assay and sequence conservation of critical residues in ARC
374 implicated in TBM binding[37], it is likely to be one of ARC2, ARC4, or ARC5.
375
376 The amino acid residues impacted by our variants are located in TBM2. Due to the ambiguity
377 regarding which ARC is responsible for TBM2 binding and the relatively low confidence in the
378 AlphaFold prediction of complex formation partners, we used the known crystal structure of the
379 TNKS/AXIN1 complex[37], in which each ARC2 of TNKS binds TBM1 and TBM2 of AXIN1,
380 respectively, as a template for our *in silico* modeling of the variant structure. The arginine side
381 chain of the mutated Gly67 was modeled using Coot. However, every rotamer conformation of
382 the arginine clashes with surrounding TNKS residues in the complex, as there is no space to
383 accommodate the bulky side chain (**Figure 2C**). As previously suggested by Morrone et al., the
384 glycine-selection gate of TNKS is crucial for binding[37]. Consequently, the large side chain of the
385 p.G67R variant of AXIN2 would prevent AXIN2 from binding.
386
387 **Figure 2D** shows the Glu66 side chain forming a hydrogen bond with the Ser363 side chain and
388 water-mediated hydrogen bonds with the main chain N-H of K362 and S363, which participate
389 in an extensive hydrogen bond network. The same hydrogen bond network, including water
390 mediated hydrogen bond interactions, was also observed in the crystal structure of ARC4 of
391 TNKS bound to a chimeric substrate peptide (PDB ID: 3TWW)[69]. These interactions would

392 become less favorable when the glutamic acid is mutated to lysine due to its positive charge.
393 The p.E66K side chain mutation model was generated using Coot, with a rotamer conformation
394 that best maintained the hydrogen bond interactions. Currently, none of the versions of
395 AlphaFold can predict water mediated interactions; therefore, relevant crystal structures were
396 used as templates to analyze the mutant structure [37,69].

397

398 **Congenital anomalies in a p.E66K founder mouse embryo screen.** We next used
399 CRISPR/Cas9 genome editing in mice to confirm the pathogenicity and associated phenotypes
400 of the p.E66K variant. Because we anticipated that the phenotypes associated with
401 heterozygosity for p.E66K in humans would lead to postnatal lethality in mice, we employed a
402 founder embryo screen (**Figure 3A**). CRISPR/Cas9-mediated HDR was used to generate
403 embryos harboring an allele with the p.E66K variant and a neighboring synonymous variant
404 (see Materials and Methods; **Figure S1**). At E18.5, embryos (n=37) were collected and each
405 screened via Sanger sequencing and Synthego ICE analysis for the contribution of wild-type,
406 indel, and p.E66K knock-in alleles (**Table S5**). Of the 37 embryos screened, 5 were wild-type
407 and 26 harbored undesired indel mutations with or without the p.E66K knock-in allele. The
408 remaining 6 embryos harbored only the p.E66K knock-in allele; however, only 2 of the 6 had
409 knock-in allele contribution at or above 50% (96% and 53% knock-in allele contribution; sense
410 and antisense ssODN targeting, respectively). Because low mosaicism for the knock-in allele
411 may not be sufficient to produce phenotypes, μCT imaging was used to phenotype only these 2
412 knock-in embryos as well as a wild-type control sibling. Both p.E66K knock-in embryos
413 displayed kinked tail and shortened soft palate abnormalities not observed in the wild-type
414 control **(Figure 3B-D**).

415

416 **Confirmation of congenital anomalies using a p.E66K N1 mouse embryo screen.** Although
417 CRISPR founder screens bypass the need to generate a mouse line for phenotyping,
418 mosaicism for the desired variant knock-in (HDR) allele, undesired indel (NHEJ) alleles, or both,
419 in founders can confound detection of genotype-phenotype relationships[70]. Thus, we sought a
420 mid-throughput approach to generate p.E66K heterozygous embryos for screening. We
421 hypothesized that a CRISPR founder animal with low mosaicism for the p.E66K allele may
422 survive to breeding age. From such an animal, N1 embryos heterozygous for the p.E66K allele
423 could be consistently generated, and genotype-phenotype associations could be more easily
424 established. To produce such a founder, we turned to prime editing, which has been shown to
425 be inefficient when editing in the mouse germline[71-74].

426

427 Using prime editing, we produced a viable male founder that was 20% mosaic for an allele
428 harboring the p.E66K variant and two neighboring synonymous variants (*Axin2*^{E66K}) (see
429 Materials and Methods; **Figure S2**). Matings using the male founder produced six litters with a
430 total of 30 liveborn N1 offspring, which were genotyped at 2-3 weeks of age. Interestingly, no
431 heterozygous *Axin2*$^{E66K/+}$ offspring were identified (**Figure 4B**). Due to these results, we
432 hypothesized that there was either no germline transmission of the p.E66K variant or the variant
433 was associated with pre-weaning lethality. Therefore, we performed *in vitro* fertilization with
434 founder sperm to determine if *Axin2*$^{E66K/+}$ N1 embryos were present and viable just prior to birth
435 (E18.5). Of 29 viable N1 embryos collected at E18.5, 14 (48%) were heterozygous for the
436 p.E66K variant allele. A Fisher's exact test comparing genotypes detected at E18.5 and weaning
437 age showed a significant difference ($p<0.0001$) (**Figure 4B**). External examination of the 14
438 *Axin2*$^{E66K/+}$ E18.5 embryos revealed kinked tail abnormalities (N=5; 36%), missing digit (N=1;
439 7%), and edema or hydrocephalus (N=2; 14%). These phenotypes were not observed in 9
440 *Axin2*$^{+/+}$ littermate controls. We performed µCT imaging on the *Axin2*$^{+/+}$ and *Axin2*$^{E66K/+}$ embryos,

441 which confirmed the observed external phenotypes (**Figure 4C&D; Figure S4**). Critically,
442 μCT imaging also revealed a shortened soft palate phenotype in all *Axin2*$^{E66K/+}$ embryos, which
443 was not observed in any *Axin2*$^{+/+}$ controls (**Figure 4D; Figure S5**). Together, the results from our
444 N1 embryo screen demonstrate that heterozygosity for *Axin2*^{E66K} causes lethality between birth
445 and weaning and embryonic phenotypes like those observed in the founder screen and in the
446 participants. Moreover, these results suggest that lethality may be secondary to the shortened
447 palate observed in *Axin2*$^{E66K/+}$ embryos.

448

449 **The p.E66K variant allele functions differently than *AXIN2* reference and pathogenic**
450 **ODCRCS variant alleles in *Drosophila*.** Although the Glu66 residue is not conserved in
451 *Drosophila melanogaster,* flies remain an important *in vivo* system for assessing variant
452 function. Hence, we generated transgenic flies that express AXIN2 reference (*AXIN2*^{REF}) or
453 variants under the control of an Upstream Activation Sequence (UAS). We generated the
454 p.E66K variant (*AXIN2*^{E66K}) present in three of the participants as well as two pathogenic
455 truncating variants (*AXIN2*^{R656X} and *AXIN2*^{W663X}) observed in oligodontia-colorectal cancer
456 syndrome (ODCRCS)[3,9]. All transgenes were inserted in the same genomic site in the flies,
457 controlling for positional effects, and ensuring similar protein expression levels (**Figure S6A**). In
458 parallel, we generated an *Axn*^{TG4} (*Axn*$^{T2A-GAL4}$) mutant *Drosophila* allele as part of a large-scale
459 resource[59]. As expected, this allele was homozygous lethal and remains lethal when *in trans*
460 with a corresponding deficiency line (*Df(3R)X3F*) lacking the *Axn* gene, indicating the *Axn*^{TG4}
461 mutant is loss-of-function. The *Axn*^{TG4} allele expresses a GAL4 transcriptional activator in the
462 same spatial and temporal pattern as the *Drosophila* gene, *Axn*. We found that expressing
463 human *AXIN2*^{REF} in heterozygous *Axn*^{TG4} flies (*Axn*$^{TG4/+}$ > *UAS- AXIN2*^{REF}/+) led to no adult flies
464 at 18°C and 22°C. These data suggested that *Axn*/*AXIN2* is likely dosage-sensitive in flies
465 which prevented us from conducting humanization-based rescue studies.

466

467 As an alternative to humanization, we turned to an overexpression-based strategy for assessing
468 the impact of reference versus variant human cDNA expression in flies in a tissue-specific
469 manner[75]. Given that AXIN2 has a known role in β-catenin-dependent Wnt signaling[17], we opted
470 to overexpress *AXIN2*^{REF} and variants in the developing wing of the fly using *nubbin-GAL4*[76]
471 where Wnt (wingless in flies) signaling is well characterized. The expression of *AXIN2*^{REF}
472 caused wing margin loss marked by posterior serration and bristle loss (**Figure 5A**). This
473 phenotype was enhanced by increasing the temperature as GAL4-mediated UAS expression of
474 the transgene is positively correlated with temperature[77] (**Figure 5A**; **Figure S6B**). Importantly,
475 overexpression of a GFP-tagged fly Axn (*Axn*^{GFP})[18] causes a similar phenotype, albeit more
476 severe. These data indicate that Axn and AXIN2 exert similar effects in the developing wing
477 disc. In this context, the *AXIN2*^{E66K} variant leads to a consistently worse phenotype than
478 *AXIN2*^{REF} as demonstrated by smaller wings as well as the presence of ectopic bristles and
479 blisters (**Figure 5A**; **Figure S6B**). These data indicate that the p.E66K may act as a gain-of-
480 function with potential neomorphic functions. The *AXIN2*^{R656X} and *AXIN2*^{W663X} variants observed
481 in ODCRCS caused an even stronger phenotype than both *AXIN2*^{REF} or *AXIN2*^{E66K} as wings
482 were smaller with more pronounced wing margin loss across temperatures. These data indicate
483 that the ODCRCS variants may also act as a gain-of-function.

484

485 To confirm that *AXIN2* overexpression impacts wingless and that downstream canonical
486 signaling (Wnt/β-catenin signaling) is affected at the cellular level, we examined the developing
487 wing disc in third instar larvae. Compared to control wing discs expressing lacZ, the expression
488 of *AXIN2*^{REF} caused a decrease in Cut staining, a Wingless downstream effector (**Figure 5B**).
489 This diminished Cut expression is further reduced when the *AXIN2*^{E66K} or the ODCRCS variants
490 are overexpressed in the developing wing disc, but only statistically significant with the

491 ODCRCS variants suggesting an intermediate function of the p.E66K variant (**Figure 5C**). In
492 line with this, the expression of Sens, a wingless responsive transcription factor expressed
493 adjacent to wingless secreting cells of the dorsal-ventral boundary is decreased in a similar
494 fashion (**Figure S7A)**. Sens expression is almost completely absent when either the *AXIN2*^{E66K}
495 or the ODCRCS variants are overexpressed in the developing wing disc (**Figure 5D**).
496 Intriguingly, the Wingless ligand is also diminished in *AXIN2*^{REF}, *AXIN2*^{E66K} and the ODCRCS
497 variants to similar degrees (**Figure 5E and Figure S7B).** These data indicate that both the
498 p.E66K and truncations observed in ODCRCS inhibit wingless signaling (WNT signaling) in this
499 tissue and can act as gain-of-function variants in this context.

500

501 To examine the impact of *AXIN2* variants in another cell context, we chose to overexpress
502 *AXIN2* in the developing *Drosophila* eye using *ey-GAL4*. Although typically a dispensable tissue
503 in flies, expression with *ey-GAL4* can sometimes lead to lethality. Here, overexpression of fly
504 *Axn*^{GFP} with *ey-GAL4* causes 100% pupal lethality at 22°C. Overexpression of *AXIN2*^{REF} or
505 *AXIN2*^{E66K} causes ~75% and ~50% pupal lethality, respectively (**Figure 6A**). In surviving
506 progeny, flies expressing *AXIN2*^{REF} display a smaller eye compared to *AXIN2*^{E66K} (**Figure 6B-C**).
507 These data suggest that when expressed in the fly eye, the p.E66K acts as a loss-of-function.
508 On the contrary, the *AXIN2*^{R656X} and *AXIN2*^{W663X} variants observed in ODCRCS cause almost
509 ~100% pupal lethality with the few survivors displaying extremely small eyes (**Figure 6C**).
510 Hence, like their function in the wing, the truncations observed in ODCRCS consistently display
511 gain-of-function activity.

512

513

514 **Discussion**

515 In this study, we identified four individuals who had previously unreported germline variants
516 (p.E66K and p.G67R) in the TNKS-binding domain of *AXIN2* and a phenotype that only partially
517 overlaps with ODCRCS, the only known Mendelian disorder associated with heterozygous
518 pathogenic variants in this gene[1-4,9,15,16]. Published phenotypes associated with germline *AXIN2*
519 variants include sparse hair and eyebrows, colonic polyps/polyposis, colorectal cancer, and
520 oligodontia or tooth agenesis[1-4,9,15,16,34]. Two recent publications suggested that cleft lip/palate,
521 olfactory neuroblastoma, and gastric adenoma should be included in the spectrum of germline
522 *AXIN2*-associated phenotypes[78,79]. In addition to several common ODCRCS phenotypes, the
523 patients in our cohort share several other overlapping phenotypes that include developmental
524 delays, microcephaly, digit and limb anomalies, ophthalmologic complications, genitourinary
525 anomalies, and unique facial features. Thus, the phenotypes caused by p.E66K and p.G67R
526 variants in *AXIN2* expand the phenotypic spectrum of AXIN2-related disorders. Pathogenic
527 variants in *AXIN2* associated with ODCRCS have been reported to impact multiple domains
528 except for the TNKS-binding domain[1-4,9,15,16,34,78]. To our knowledge, these two variants
529 described here are the first *AXIN2* pathogenic variants that impact the TNKS-binding domain.

530

531 Relative to ODCRCS, the more severe phenotypes of our patients with p.E66K or p.G67R
532 variants suggest the variants in the TNKS-binding domain of AXIN2 have a unique impact on
533 AXIN2 function. TNKS poly-ADP-ribosylates AXIN2, which leads to the ubiquitination and
534 proteasomal degradation of AXIN2[35,37]. Our structural modeling studies suggest that these
535 variants may directly impact TNKS binding to AXIN2. In particular, the p.G67R variant is
536 predicted to completely abolish AXIN2 binding to TNKS, while the p.E66K variant is predicted to
537 weaken the interaction with the main chain N-H of K362/S363 due to a less favorable charge
538 distribution, although a polar interaction with Serine 363 is still possible. In vitro studies of a
539 p.G74V mutation in AXIN1 (which is equivalent to p.G67V in AXIN2) demonstrated that this

540 mutation prevents TNKS from binding to AXIN1 in GST-pulldown assays, a finding that supports
541 our data[37]. Thus, a p.E66K or p.G67R variant may prevent TNKS and AXIN2 binding, which may
542 lead to increased stability of AXIN2.

543

544 The modeling of *de novo* heterozygous variants associated with severe early-onset phenotypes
545 is challenging in mice using traditional constitutive knock-in strategies due to expected lethality.
546 Thus, to circumvent this challenge, we used two mouse embryo screening approaches to
547 confirm the pathogenicity and phenotypes of the p.E66K variant, which was identified in 3 of the
548 4 participants in our cohort. Using both a CRISPR founder embryo screen and an innovative
549 prime editing N1 embryo screen, the p.E66K variant was found to cause shortened soft palate,
550 kinked tail, and digit abnormalities, phenotypes resembling the palate and skeletal abnormalities
551 observed in the participants. Moreover, the observed perinatal lethality of N1 mice heterozygous
552 for the p.E66K variant further supported pathogenicity. Given that the soft palate elevates during
553 swallowing to prevent food and fluids from going into the nasopharynx, we propose that p.E66K
554 heterozygous pups die shortly after birth due to nasal regurgitation. Importantly, the phenotypes
555 observed in mouse embryos heterozygous for the p.E66K variant contrast with the those in
556 published reports describing *Axin2* homozygous knockout mice, which are viable, fertile, and
557 have abnormal cranial suture closure[13,80-82]. This suggests that the effect of the p.E66K variant
558 on AXIN2 function is not simply loss-of-function.

559

560 Our fly modeling supports a complex and cell context-dependent effect of the p.E66K mutation
561 on AXIN2 function. Overexpression of the p.E66K and ODCRCS variant alleles caused more
562 severe phenotypes than overexpression of reference AXIN2 in the fly wing, indicating gain-of-
563 function for all variants tested. Overexpression of the p.E66K variant in the developing fly wing

564 also caused ectopic bristles, which were not observed in reference or ODCRCS variant
565 expressing wings, indicating potential neomorphic activity. In contrast, overexpression of the
566 p.E66K variant in the developing *Drosophila* eye caused less severe phenotypes compared to
567 reference, which is consistent with AXIN2 loss-of-function. Critically, overexpression of the
568 ODCRCS variants in the eye produced phenotypes consistent with AXIN2 gain-of-function, like
569 their overexpression in the wing. Thus, the effect of the p.E66K variant on AXIN2 function is
570 complex, context-dependent, and different than the ODCRCS variants, revealing a potential
571 underlying mechanism for phenotypic expansion.

572

573 *In vitro*, many ODCRCS variants produce premature stop codons distributed throughout *AXIN2*,
574 but some of these mutant transcripts appear to escape nonsense-mediated decay[83].
575 Consequently, truncated AXIN2 protein is produced, retains AXIN2 function, and demonstrates
576 increased stability in some situations[83]. These molecular characteristics are consistent with the
577 gain-of-function phenotypes observed when these variants are overexpressed in both the fly
578 wing and eye. Why the p.E66K variant in the TNKS binding domain revealed differential, cell
579 context-specific effects on AXIN2 function (i.e., gain-of-function versus loss-of-function) in our fly
580 models remains to be resolved. Cell context-specific roles for TNKS in the regulation of AXIN2
581 protein levels could play a role.

582

583 The function of AXIN2 in canonical Wnt signaling is primarily considered to be inhibitory, as
584 AXIN2 is a critical component of the β-catenin destruction complex in the absence of Wnt
585 signaling. However, once Wnt signaling is active, AXIN2 binds to and plays an important role in
586 maintaining the phosphorylation of the Lrp5/6 receptors, effectively promoting Wnt signaling[29-32].
587 The phenotypes observed in our mouse and fly models support this dichotomous role for AXIN2

588 in canonical Wnt signaling, which may also be cell context-dependent. Canonical Wnt/β-catenin
589 signaling in cranial neural crest (CNC)-derived mesenchymal cells is essential for proper
590 development of the soft palate, and the shortened soft palate phenotype in p.E66K
591 heterozygous embryos is consistent with disruption of Wnt signaling in these cells[84,85]. On the
592 other hand, the kinked tail phenotype observed in p.E66K heterozygous embryos is consistent
593 with hyperactivation of Wnt signaling in the neural tube[86]. Interestingly, previous studies of
594 mouse embryos harboring an ENU-induced p.V26D mutation in the tankyrase binding domain of
595 *Axin2* (*Axin2*^{canp}, **Figure S3**) revealed similar cell context-dependent effects with inhibition of
596 Wnt signaling in many embryonic tissues but a gain of Wnt signaling in the primitive streak[36].
597 Similarly, the phenotypes caused by AXIN2 overexpressed in the *Drosophila* wing are consistent
598 with inhibition of Wnt signaling[61,87]; the phenotypes induced by AXIN2 overexpressed in the
599 *Drosophila* eye are suggestive of Wnt signaling activation as Wnt plays an inhibitory role in
600 Drosophila eye development[88].

601

602 Based on patient phenotypes and our animal modeling data, we propose that specific variants
603 impacting the TNKS-binding domain of AXIN2 are associated with phenotypic expansion and a
604 novel Mendelian disorder with an underlying complex molecular mechanism. Future studies will
605 explore the cell context-specific effects of TNKS-binding domain variants on AXIN2 stability,
606 AXIN2 function, and Wnt/β-catenin signaling. The modeling strategies used to demonstrate the
607 pathogenicity of this variant may be beneficial for the resolution of other *de novo* heterozygous
608 variants of uncertain significance associated with congenital anomalies in humans.

609

610 **Declaration of Interests**

611 The Department of Molecular and Human Genetics at Baylor College of Medicine receives
612 financial support from Baylor Genetics. Dr. Brendan Lee serves on the Board of Directors of
613 Baylor Genetics and chairs its Scientific Advisory Board but receives no personal income from
614 these positions. XH is an employee of and may hold stock in GeneDx, LLC.

615

616

617 **Acknowledgements**

618 We thank the patients and families for participating in this study. Clinical research reported in
619 this publication was supported in part by National Institutes of Health (NIH) U01HG007709 to BL
620 and U01NS134348 to BL and JR. The genome sequencing for participant 1 was done through
621 the UDN Clinical Sequencing Core supported by NIH U01HG007942. Use of the Baylor College
622 of Medicine Intellectual and Developmental Disabilities Research Center Clinical translational
623 core was supported by P50HD103555. Fly modeling was supported by NIH U54NS093793,
624 R24OD022005, and R24OD031447 to HJB, OK and SY**.** Mouse modeling was supported by
625 NIH U54OD030165 to JDH and LCB. Use of the Macromolecular X-ray Crystallography Core at
626 Baylor College of Medicine was supported in part by NIH S10OD030246 to SL. Use of the
627 Optical Imaging & Vital Microscopy Core at the Baylor College of Medicine and the MicroCT
628 Imaging Facility at the McGovern Medical School at UTHealth was supported in part by NIH
629 S10OD030336. Use of the BCM Genetically Engineered Rodent Models Core was supported in
630 part by the Dan L. Duncan Comprehensive Cancer Center Support grant P30CA125123. The
631 content is solely the responsibility of the authors and does not necessarily represent the official
632 views of the National Institutes of Health. The mention of trade names, commercial products, or
633 organizations do not imply endorsement by the US Government. LCB and HTC are supported
634 by a Burroughs Wellcome Fund Career Award for Medical Scientists. HTC is supported by the

635 Cain Pediatric Neurology Research Foundation Laboratories and McNair Medical Institute at
636 The Robert and Janice McNair Foundation.

637

638 **Figure List**:

639 **Figure 1**. **Participant Phenotypes.** A) Pathogenic germline variants identified in *AXIN2*. The
640 variants we identified are shown in red, previously published variants associated with
641 oligodontia, oligodontia colorectal cancer syndrome, colon cancer and colon polyps previously
642 published are shown in black[1-4,15,16]. TNKS = Tankyrase binding domain, RGS = Regulator of G-
643 protein Signaling domain, GSK3β = Glycogen synthase kinase-3 beta binding domain, β-CAT =
644 Beta-catenin binding domain, DIX = Disheveled and AXIN (DIX) dimerization domain. B) *AXIN2*
645 missense allele counts derived from gnomAD aligned to human and mouse AXIN2 and AXIN1
646 amino acid alignments. Amino acids highlighted in red are conserved between all aligned
647 proteins, and positions 66 and 67 are highlighted in blue. The absence of variation in gnomAD
648 at positions 65 through 67 suggests that these residues may be critical for proper function of
649 AXIN2. Conservation alignment was created using default parameters in Clustal Omega[43].
650 Amino acids 60-75 from AXIN2 are shown, and amino acids 67-82 from AXIN1 are shown.
651 Variant allele counts were compiled from gnomAD_v4.0.0_ENSG00000168646_2.

652

653 **Figure 2**. **Structural Model of the AXIN2 variants.** A) ARC2 of TNKS is shown as a stick
654 model and surface representation. View looking from inside of the molecule toward the surface.
655 B) Bound TBM2 of AXIN2 is shown in stick and surface representation and is colored in green.
656 C) Bound TBM2 of the AXIN2 variant is shown in magenta. Enlarged view of the p.G67R mutant
657 showing steric clashes with surrounding residues. D) The Glu66 side chain of AXIN2 TBM2
658 (green) participates in an extensive hydrogen bond network (dotted red line) that stabilizes

659 complex formation. This hydrogen bond network would be disrupted by p.E66K mutation
660 (yellow). Water molecules are shown in red balls. The model was generated based on the
661 crystal structure of AXIN1 bound to TNKS (PDB ID: 3UTM).

662

663 **Figure 3**. **Production, genotyping, and phenotyping of p.E66K founder embryos.** A)
664 Outline of the process for generating and screening CRISPR founder embryos. B-D) Internal
665 and external µCT images of embryos at E18.5 with respective Sanger sequence traces. B) A
666 representative wild type embryo from the founder screen. No external anomalies are present
667 (left images), and the soft palate is the expected length (right images). C) Embryo with 96%
668 p.E66K knock-in allele contribution. This embryo had a kinked tail (left images) and had a
669 shortened soft palate not extending to the epiglottis (right images). D) Embryo with 53% p.E66K
670 knock-in allele contribution. This embryo also has a kinked tail (left images) and a shortened
671 soft palate (right images). Bottom images are magnified views of the areas in red boxes on the
672 top images. Arrowhead indicates normal soft palate extending to the epiglottis. Arrows indicate
673 shortened soft palates.

674

675 **Figure 4. Production, genotyping, and phenotyping of the p.E66K knock-in mouse model.**
676 A) Outline of the mosaic founder production and N1 screen for the p.E66K knock-in allele
677 generated with prime editing. B) Genotype distribution of N1 E18.5 embryos and liveborn
678 animals generated from the p.E66K mosaic founder. There were no N1 *Axin2*$^{E66K/+}$ animals at
679 weaning age, whereas about 50% of the embryos at E18.5 were carriers ($p < 0.0001$, Fisher's
680 exact for genotype distribution across timepoints). C) A representative E18.5 wild type embryo
681 from the N1 screen. No external anomalies are present (left images), and the soft palate is the
682 expected length, extending to the epiglottis (right images). D) A representative E18.5 *Axin2*$^{E66K/+}$

683 embryo with missing forelimb 5th digit (left images) and edema and a shortened soft palate not
684 extending to the epiglottis (right images). Bottom images are magnified views of the areas in red
685 boxes on the top images. Dashed arrow indicates edema. Arrowhead indicates normal soft
686 palate extending to the epiglottis. Arrows indicate missing digit and shortened soft palate.

687

688 **Figure 5. The p.E66K acts as a gain-of-function variant in the *Drosophila* wing.** A)
689 Representative images of adult fly wings expressing UAS-cDNA using *nubbin-GAL4* at the
690 temperatures indicated. A minimum of 60 wings were examined from three independent
691 crosses. Phenotypes were nearly 100% penetrant. B) Representative immunostaining of the Cut
692 protein in the developing wing disc at 22°C upon UAS-cDNA overexpression with *nubbin-GAL4*.
693 Scale bar = 40 μm. C-E) Quantification of fluorescence signal for Cut, Sens, and Wingless (Wg)
694 proteins in the developing wing disc upon overexpression of UAS-cDNA using *nubbin-GAL4* at
695 22°C. Immunostaining images for Sens and Wg are provided in Figure S7. ANOVA followed by
696 Tukey's post hoc test. *p<0.05, **p<0.01, ***p<0.001, ****p<0.0001.

697

698 **Figure 6. The p.E66K acts as a loss-of-function variant in the *Drosophila* eye.** A)
699 Quantification of pupal lethality upon overexpression of UAS-cDNA with ey-GAL4 at 22°C.
700 ANOVA followed by Tukey's post hoc test. ****p<0.0001. B) Range of eye phenotypes identified
701 upon overexpression of UAS-cDNA with *ey-GAL4* at 22°C in surviving adult flies. C)
702 Representative images of eye phenotypes upon overexpression of UAS-cDNA with *ey-GAL4* at
703 22°C in surviving adult flies.

704

705 **<u>Supplemental Material</u>**

706 **Supplemental Figures**

707 **Figure S1. Genome editing approaches for the p.E66K founder embryos.** A) Genome
708 editing with a sense strand derived sgRNA and anti-sense strand derived ssODN. B) Genome
709 editing with a sense strand derived sgRNA and anti-sense strand derived ssODN. Scissors
710 indicate sgRNA cut sites; asterisks indicate p.E66K mutation and p.G67 synonymous mutation.
711 The location of primers (E2 F and E2 R) used for PCR genotyping and Sanger sequencing are
712 shown.

713

714 **Figure S2. Production and characterization of *Axin2*$^{E66K/+}$ mosaic founder and N1**
715 **embryos.** A) Prime editing production of a mosaic founder. Orange scissors indicate the
716 pegRNA; green scissors indicate the sgRNA for DNA nicking. The asterisk indicates p.E66K
717 mutation and p.G67 synonymous mutation. Insertion of the p.E66K mutation generates a StyI
718 restriction endonuclease cut site. The location of primers (E2 F and E2 R) used for PCR
719 genotyping and Sanger sequencing are shown. The 653 bp wild type PCR product is not
720 digested by StyI; the 653 bp p.E66K variant allele PCR products are digested by StyI, resulting
721 in 335 and 318 bp products. B) Sanger sequencing traces of the mosaic founder, a
722 representative Axin2$^{E66K/+}$ N1 embryo, and a representative wild type N1 embryo. The founder
723 male is mosaic for an allele harboring the p.E66K point mutation, a p.G67 synonymous
724 mutation, and a p.S70 (TCG>TCC) synonymous mutation. Co-transmission of the variants to N1
725 offspring confirms linkage. C) Representative PCR-StyI restriction digest genotyping results for
726 N1 embryos. NTC = no template control.

727

728 **Figure S3**. **Extended gnomAD conservation figure and *AXIN2* conservation across**
729 **multiple species.** A) Conservation alignment between *Homo sapiens* AXIN2, *Drosophila*

730 *melanogaster* AXN, and AXIN2 from various organisms (see methods and materials for full list).
731 Amino acids highlighted in red are 90-100% identical in the alignment, orange is 80-89%
732 identical, yellow is 70-79% identical. Positions 66 and 67 in human AXIN2 are highlighted in
733 blue, p.E66 and p.G67 are conserved in all organisms aligned except *D. melanogaster*. B)
734 *AXIN2* missense allele counts derived from gnomAD aligned to *Homo sapiens* and *Mus*
735 *musculus* AXIN2, and *Homo sapiens* and *Mus musculus* AXIN1. Red color highlights amino
736 acids conserved between all aligned proteins, positions 66 and 67 are highlighted in blue. The
737 absence of variation in gnomAD at positions 65 through 67 suggests that these residues may be
738 critical for proper function of AXIN2. Missense variant allele counts were compiled from
739 gnomAD_v4.0.0_ENSG00000168646_2.

740

741 **Figure S4. External imaging of embryos from the N1 screen.** External µCT images of E18.5
742 wild type (WT, *Axin2*$^{+/+}$) and p.E66K heterozygous (Het, *Axin2*$^{E66K/+}$) embryos from the N1
743 screen. No external anomalies are present in wild type embryos; missing digit (N1-19) and
744 kinked tail phenotypes (N1-11, 15, 16, 22, 23) are observed in *Axin2*$^{E66K/+}$ embryos (arrows).

745

746 **Figure S5. Internal imaging of embryos from the N1 screen.** Internal, sagittal µCT images of
747 E18.5 wild type (*Axin2*$^{+/+}$) and p.E66K heterozygous (*Axin2*$^{E66K/+}$) embryos from the N1 screen.
748 No internal anomalies are present in wild type embryos, with the soft palate extending to the
749 epiglottis (box); all *Axin2*$^{E66K/+}$ embryos have a shortened soft palate not extending to the
750 epiglottis (box).

751

752 **Figure S6. The p.E66K variant is stable and acts as a gain-of-function variant in the**
753 ***Drosophila* wing.** A) Representative western blot showing expression of UAS-AXIN2 cDNA

754 constructs are stable and relatively similar in level. B) Representative images of adult fly wings
755 expressing UAS-cDNA using *nubbin-GAL4* at the temperatures indicated. A minimum of 60
756 wings were examined from three independent crosses. Phenotypes were nearly 100%
757 penetrant.

758

759 **Figure S7. The p.E66K variant leads to increased inhibition of Wingless signaling.** A-B)
760 Representative immunostaining of the Sens and Wg protein in the developing wing disc at 22°C
761 upon UAS-cDNA overexpression with *nubbin-GAL4*. Scale bar = 40 μm.

762

763 **Supplemental Tables**

764 **Table S1** – Guides for *Axin2* founder screen by traditional CRISPR HDR.

765 **Table S2** – T Guides for Axin2 mouse model production by prime editing.

766 **Table S3** – Prime editing pegRNA sequences.

767 **Table S4** – Primers used for site-directed mutagenesis of AXIN2 for fly modeling.

768 **Table S5** – Results of the ICE analysis of Sanger sequencing reads from p.E66K founder embryos.

769

770 **Member Lists**

771 Members of the UDN and members of the BCM CPMM lists are provided in supplemental material.

772
773 **Web Resources**:
774
775 AlphaFold2 Multimer, https://github.com/sokrypton/ColabFold
776 AlphaFold3, https://alphafoldserver.com
777 CADD, https://cadd.gs.washington.edu/
778 Catalogue of Somatic Mutations in Cancer (COSMIC), https://cancer.sanger.ac.uk/cosmic
779 Clinvar, https://www.ncbi.nlm.nih.gov/clinvar/

Clustal Omega, http://www.clustal.org/
Codified Genomics, https://codifiedgenomics.com
Developmental Studies Hybridoma Bank, https://dshb.biology.uiowa.edu/
Gnomad, https://gnomad.broadinstitute.org/
OMIM, https://www.omim.org/
Mouse Genome Informatics (MGI), https://www.informatics.jax.org/
Pegfinder, http://pegfinder.sidichenlab.org
REVEL, https://sites.google.com/site/revelgenomics/
Wellcome Sanger Institute Genome Editing (WGE), https://wge.stemcell.sanger.ac.uk/
Synthego Inference of CRISPR Edits (ICE), https://ice.synthego.com/#/

References

1. Beard, C., Purvis, R., Winship, I.M., Macrae, F.A., and Buchanan, D.D. (2019). Phenotypic confirmation of oligodontia, colorectal polyposis and cancer in a family carrying an exon 7 nonsense variant in the AXIN2 gene. Familial Cancer *18*, 311-315. 10.1007/s10689-019-00120-0.
2. Jensen, J.M., Skakkebæk, A., Gaustadness, M., Sommerlund, M., Gjørup, H., Ljungmann, K., Lautrup, C.K., and Sunde, L. (2022). Familial colorectal cancer and tooth agenesis caused by an AXIN2 variant: how do we detect families with rare cancer predisposition syndromes? Familial Cancer *21*, 325-332. 10.1007/s10689-021-00280-y.
3. Lammi, L., Arte, S., Somer, M., Järvinen, H., Lahermo, P., Thesleff, I., Pirinen, S., and Nieminen, P. (2004). Mutations in AXIN2 Cause Familial Tooth Agenesis and Predispose to Colorectal Cancer. The American Journal of Human Genetics *74*, 1043-1050. 10.1086/386293.
4. Yue, H., Liang, J., Yang, K., Hua, B., and Bian, Z. (2016). Functional analysis of a novel missense mutation in AXIN2 associated with non-syndromic tooth agenesis. European Journal of Oral Sciences *124*, 228-233. https://doi.org/10.1111/eos.12273.
5. Arenas, E. (2014). Wnt signaling in midbrain dopaminergic neuron development and regenerative medicine for Parkinson's disease. Journal of Molecular Cell Biology *6*, 42-53. 10.1093/jmcb/mju001.
6. Jia, L., Piña-Crespo, J., and Li, Y. (2019). Restoring Wnt/β-catenin signaling is a promising therapeutic strategy for Alzheimer's disease. Molecular Brain *12*, 104. 10.1186/s13041-019-0525-5.
7. Wang, Q., Huang, X., Su, Y., Yin, G., Wang, S., Yu, B., Li, H., Qi, J., Chen, H., Zeng, W., et al. (2022). Activation of Wnt/β-catenin pathway mitigates blood–brain barrier dysfunction in Alzheimer's disease. Brain *145*, 4474-4488. 10.1093/brain/awac236.
8. Lancaster, M.A., Louie, C.M., Silhavy, J.L., Sintasath, L., DeCambre, M., Nigam, S.K., Willert, K., and Gleeson, J.G. (2009). Impaired Wnt–β-catenin signaling disrupts adult renal homeostasis and leads to cystic kidney ciliopathy. Nature Medicine *15*, 1046-1054. 10.1038/nm.2010.
9. Marvin, M.L., Mazzoni, S.M., Herron, C.M., Edwards, S., Gruber, S.B., and Petty, E.M. (2011). AXIN2-associated autosomal dominant ectodermal dysplasia and neoplastic syndrome. American Journal of Medical Genetics Part A *155*, 898-902. https://doi.org/10.1002/ajmg.a.33927.
10. Yook, J.I., Li, X.-Y., Ota, I., Hu, C., Kim, H.S., Kim, N.H., Cha, S.Y., Ryu, J.K., Choi, Y.J., Kim, J., et al. (2006). A Wnt–Axin2–GSK3β cascade regulates Snail1 activity in breast cancer cells. Nature Cell Biology *8*, 1398-1406. 10.1038/ncb1508.

11. Liu, J., Xiao, Q., Xiao, J., Niu, C., Li, Y., Zhang, X., Zhou, Z., Shu, G., and Yin, G. (2022). Wnt/β-catenin signalling: function, biological mechanisms, and therapeutic opportunities. Signal Transduction and Targeted Therapy *7*, 3. 10.1038/s41392-021-00762-6.
12. Satoh, S., Daigo, Y., Furukawa, Y., Kato, T., Miwa, N., Nishiwaki, T., Kawasoe, T., Ishiguro, H., Fujita, M., Tokino, T., et al. (2000). AXIN1 mutations in hepatocellular carcinomas, and growth suppression in cancer cells by virus-mediated transfer of AXIN1. Nature Genetics *24*, 245-250. 10.1038/73448.
13. Lustig, B., Jerchow, B., Sachs, M., Weiler, S., Pietsch, T., Karsten, U., van de Wetering, M., Clevers, H., Schlag, P.M., Birchmeier, W., and Behrens, J. (2002). Negative Feedback Loop of Wnt Signaling through Upregulation of Conductin/Axin2 in Colorectal and Liver Tumors. Molecular and Cellular Biology *22*, 1184-1193. 10.1128/MCB.22.4.1184-1193.2002.
14. Korinek, V., Barker, N., Morin, P.J., van Wichen, D., de Weger, R., Kinzler, K.W., Vogelstein, B., and Clevers, H. (1997). Constitutive Transcriptional Activation by a β-Catenin-Tcf Complex in APC−/− Colon Carcinoma. Science *275*, 1784-1787. 10.1126/science.275.5307.1784.
15. Chan, J.M., Clendenning, M., Joseland, S., Georgeson, P., Mahmood, K., Walker, R., Como, J., Joo, J.E., Preston, S., Hutchinson, R.A., et al. (2022). Rare germline variants in the AXIN2 gene in families with colonic polyposis and colorectal cancer. Familial Cancer *21*, 399-413. 10.1007/s10689-021-00283-9.
16. Leclerc, J., Beaumont, M., Vibert, R., Pinson, S., Vermaut, C., Flament, C., Lovecchio, T., Delattre, L., Demay, C., Coulet, F., et al. (2023). AXIN2 germline testing in a French cohort validates pathogenic variants as a rare cause of predisposition to colorectal polyposis and cancer. Genes, Chromosomes and Cancer *62*, 210-222. https://doi.org/10.1002/gcc.23112.
17. Wu, Z.-Q., Brabletz, T., Fearon, E., Willis, A.L., Hu, C.Y., Li, X.-Y., and Weiss, S.J. (2012). Canonical Wnt suppressor, Axin2, promotes colon carcinoma oncogenic activity. Proceedings of the National Academy of Sciences *109*, 11312-11317. 10.1073/pnas.1203015109.
18. Cliffe, A., Hamada, F., and Bienz, M. (2003). A Role of Dishevelled in Relocating Axin to the Plasma Membrane during Wingless Signaling. Current Biology *13*, 960-966. 10.1016/S0960-9822(03)00370-1.
19. Ikeda, S., Kishida, S., Yamamoto, H., Murai, H., Koyama, S., and Kikuchi, A. (1998). Axin, a negative regulator of the Wnt signaling pathway, forms a complex with GSK-3β and β-catenin and promotes GSK-3β-dependent phosphorylation of β-catenin. The EMBO Journal *17*, 1371-1384-1384. https://doi.org/10.1093/emboj/17.5.1371.
20. Jho, E.-h., Zhang, T., Domon, C., Joo, C.-K., Freund, J.-N., and Costantini, F. (2002). Wnt/β-Catenin/Tcf Signaling Induces the Transcription of Axin2, a Negative Regulator of the Signaling Pathway. Molecular and Cellular Biology *22*, 1172-1183. 10.1128/MCB.22.4.1172-1183.2002.
21. Zeng, X., Huang, H., Tamai, K., Zhang, X., Harada, Y., Yokota, C., Almeida, K., Wang, J., Doble, B., Woodgett, J., et al. (2008). Initiation of Wnt signaling: control of Wnt coreceptor Lrp6 phosphorylation/activation via frizzled, dishevelled and axin functions. Development *135*, 367-375. 10.1242/dev.013540.
22. Rubinfeld, B., Albert, I., Porfiri, E., Fiol, C., Munemitsu, S., and Polakis, P. (1996). Binding of GSK3β to the APC-β-Catenin Complex and Regulation of Complex Assembly. Science *272*, 1023-1026. 10.1126/science.272.5264.1023.
23. Orford, K., Crockett, C., Jensen, J.P., Weissman, A.M., and Byers, S.W. (1997). Serine Phosphorylation-regulated Ubiquitination and Degradation of β-Catenin*. Journal of Biological Chemistry *272*, 24735-24738. https://doi.org/10.1074/jbc.272.40.24735.

24. Hart, M., Concordet, J.P., Lassot, I., Albert, I., del los Santos, R., Durand, H., Perret, C., Rubinfeld, B., Margottin, F., Benarous, R., and Polakis, P. (1999). The F-box protein β-TrCP associates with phosphorylated β-catenin and regulates its activity in the cell. Current Biology *9*, 207-211. 10.1016/S0960-9822(99)80091-8.
25. Aberle, H., Bauer, A., Stappert, J., Kispert, A., and Kemler, R. (1997). β-catenin is a target for the ubiquitin-proteasome pathway. The EMBO journal *16*, 3797-3804. 10.1093/emboj/16.13.3797.
26. Behrens, J., von Kries, J.P., Kühl, M., Bruhn, L., Wedlich, D., Grosschedl, R., and Birchmeier, W. (1996). Functional interaction of β-catenin with the transcription factor LEF-1. Nature *382*, 638-642. 10.1038/382638a0.
27. Molenaar, M., van de Wetering, M., Oosterwegel, M., Peterson-Maduro, J., Godsave, S., Korinek, V., Roose, J., Destrée, O., and Clevers, H. (1996). XTcf-3 Transcription Factor Mediates β-catenin-Induced Axis Formation in Xenopus Embryos. Cell *86*, 391-399. 10.1016/S0092-8674(00)80112-9.
28. (!!! INVALID CITATION !!! 28-30).
29. Zeng, X., Huang, H., Tamai, K., Zhang, X., Harada, Y., Yokota, C., Almeida, K., Wang, J., Doble, B., Woodgett, J., et al. (2008). Initiation of Wnt signaling: control of Wnt coreceptor Lrp6 phosphorylation/activation via frizzled, dishevelled and axin functions. Development *135*, 367-375. 10.1242/dev.013540.
30. Mao, J., Wang, J., Liu, B., Pan, W., Farr, G.H., 3rd, Flynn, C., Yuan, H., Takada, S., Kimelman, D., Li, L., and Wu, D. (2001). Low-density lipoprotein receptor-related protein-5 binds to Axin and regulates the canonical Wnt signaling pathway. Mol Cell *7*, 801-809. 10.1016/s1097-2765(01)00224-6.
31. Zeng, X., Tamai, K., Doble, B., Li, S., Huang, H., Habas, R., Okamura, H., Woodgett, J., and He, X. (2005). A dual-kinase mechanism for Wnt co-receptor phosphorylation and activation. Nature *438*, 873-877. 10.1038/nature04185.
32. Bilic, J., Huang, Y.L., Davidson, G., Zimmermann, T., Cruciat, C.M., Bienz, M., and Niehrs, C. (2007). Wnt induces LRP6 signalosomes and promotes dishevelled-dependent LRP6 phosphorylation. Science *316*, 1619-1622. 10.1126/science.1137065.
33. Liu, W., Dong, X., Mai, M., Seelan, R.S., Taniguchi, K., Krishnadath, K.K., Halling, K.C., Cunningham, J.M., Qian, C., Christensen, E., et al. (2000). Mutations in AXIN2 cause colorectal cancer with defective mismatch repair by activating β-catenin/TCF signalling. Nature Genetics *26*, 146-147. 10.1038/79859.
34. Bergendal, B., Klar, J., Stecksén-Blicks, C., Norderyd, J., and Dahl, N. (2011). Isolated oligodontia associated with mutations in EDARADD, AXIN2, MSX1, and PAX9 genes. American Journal of Medical Genetics Part A *155*, 1616-1622. https://doi.org/10.1002/ajmg.a.34045.
35. Huang, S.-M.A., Mishina, Y.M., Liu, S., Cheung, A., Stegmeier, F., Michaud, G.A., Charlat, O., Wiellette, E., Zhang, Y., Wiessner, S., et al. (2009). Tankyrase inhibition stabilizes axin and antagonizes Wnt signalling. Nature *461*, 614-620. 10.1038/nature08356.
36. Qian, L., Mahaffey, J.P., Alcorn, H.L., and Anderson, K.V. (2011). Tissue-specific roles of Axin2 in the inhibition and activation of Wnt signaling in the mouse embryo. Proceedings of the National Academy of Sciences *108*, 8692-8697. 10.1073/pnas.1100328108.
37. Morrone, S., Cheng, Z., Moon, R.T., Cong, F., and Xu, W. (2012). Crystal structure of a Tankyrase-Axin complex and its implications for Axin turnover and Tankyrase substrate recruitment. Proceedings of the National Academy of Sciences *109*, 1500-1505. doi:10.1073/pnas.1116618109.

38. Landrum, M.J., Lee, J.M., Riley, G.R., Jang, W., Rubinstein, W.S., Church, D.M., and Maglott, D.R. (2014). ClinVar: public archive of relationships among sequence variation and human phenotype. Nucleic Acids Research *42*, D980-D985. 10.1093/nar/gkt1113.
39. Yang, Y., Muzny, D.M., Xia, F., Niu, Z., Person, R., Ding, Y., Ward, P., Braxton, A., Wang, M., Buhay, C., et al. (2014). Molecular findings among patients referred for clinical whole-exome sequencing. JAMA *312*, 1870-1879. 10.1001/jama.2014.14601.
40. Keehan, L., Jiang, M.M., Li, X., Marom, R., Dai, H., Murdock, D., Liu, P., Hunter, J.V., Heaney, J.D., Robak, L., et al. (2021). A novel de novo intronic variant in ITPR1 causes Gillespie syndrome. Am J Med Genet A *185*, 2315-2324. 10.1002/ajmg.a.62232.
41. Chen, S., Francioli, L.C., Goodrich, J.K., Collins, R.L., Kanai, M., Wang, Q., Alföldi, J., Watts, N.A., Vittal, C., Gauthier, L.D., et al. (2022). A genome-wide mutational constraint map quantified from variation in 76,156 human genomes. bioRxiv, 2022.2003.2020.485034-482022.485003.485020.485034. 10.1101/2022.03.20.485034.
42. Goujon, M., McWilliam, H., Li, W., Valentin, F., Squizzato, S., Paern, J., and Lopez, R. (2010). A new bioinformatics analysis tools framework at EMBL–EBI. Nucleic Acids Research *38*, W695-W699. 10.1093/nar/gkq313.
43. Sievers, F., Wilm, A., Dineen, D., Gibson, T.J., Karplus, K., Li, W., Lopez, R., McWilliam, H., Remmert, M., Söding, J., et al. (2011). Fast, scalable generation of high-quality protein multiple sequence alignments using Clustal Omega. Molecular Systems Biology *7*, 539. https://doi.org/10.1038/msb.2011.75.
44. Söding, J. (2005). Protein homology detection by HMM–HMM comparison. Bioinformatics *21*, 951-960. 10.1093/bioinformatics/bti125.
45. UniProt, C. (2023). UniProt: the Universal Protein Knowledgebase in 2023. Nucleic Acids Res *51*, D523-D531. 10.1093/nar/gkac1052.
46. Emsley, P., Lohkamp, B., Scott, W.G., and Cowtan, K. (2010). Features and development of Coot. Acta Crystallogr D Biol Crystallogr *66*, 486-501. 10.1107/S0907444910007493.
47. Hodgkins, A., Farne, A., Perera, S., Grego, T., Parry-Smith, D.J., Skarnes, W.C., and Iyer, V. (2015). WGE: a CRISPR database for genome engineering. Bioinformatics *31*, 3078-3080. 10.1093/bioinformatics/btv308.
48. Lanza, D.G., Mao, J., Lorenzo, I., Liao, L., Seavitt, J.R., Ljungberg, M.C., Simpson, E.M., DeMayo, F.J., and Heaney, J.D. (2024). An oocyte-specific Cas9-expressing mouse for germline CRISPR/Cas9-mediated genome editing. genesis *62*, e23589. https://doi.org/10.1002/dvg.23589.
49. Chow, R.D., Chen, J.S., Shen, J., and Chen, S. (2021). A web tool for the design of prime-editing guide RNAs. Nat Biomed Eng *5*, 190-194. 10.1038/s41551-020-00622-8.
50. Hai, L., Szwarc, M.M., Lanza, D.G., Heaney, J.D., and Lydon, J.P. (2019). Using CRISPR/Cas9 engineering to generate a mouse with a conditional knockout allele for the promyelocytic leukemia zinc finger transcription factor. genesis *57*, e23281. https://doi.org/10.1002/dvg.23281.
51. Nakao, K., Nakagata, N., and Katsuki, M. (1997). Simple and Efficient Vitrification Procedure for Cryopreservation of Mouse Embryos. Experimental Animals *46*, 231-234. 10.1538/expanim.46.231.
52. Nakagata, N., and Takeo, T. (2019). Basic mouse reproductive techniques developed and modified at the Center for Animal Resources and Development (CARD), Kumamoto University. Experimental Animals *68*, 391-395. 10.1538/expanim.19-0070.
53. Dickinson, M.E., Flenniken, A.M., Ji, X., Teboul, L., Wong, M.D., White, J.K., Meehan, T.F., Weninger, W.J., Westerberg, H., Adissu, H., et al. (2016). High-throughput discovery of novel developmental phenotypes. Nature *537*, 508-514. 10.1038/nature19356.

54. Takeo, T., Hoshii, T., Kondo, Y., Toyodome, H., Arima, H., Yamamura, K.-i., Irie, T., and Nakagata, N. (2008). Methyl-Beta-Cyclodextrin Improves Fertilizing Ability of C57BL/6 Mouse Sperm after Freezing and Thawing by Facilitating Cholesterol Efflux from the Cells1. Biology of Reproduction *78*, 546-551. 10.1095/biolreprod.107.065359.
55. Takeo, T., and Nakagata, N. (2011). Reduced Glutathione Enhances Fertility of Frozen/Thawed C57BL/6 Mouse Sperm after Exposure to Methyl-Beta-Cyclodextrin1. Biology of Reproduction *85*, 1066-1072. 10.1095/biolreprod.111.092536.
56. Chung, H.L., Mao, X., Wang, H., Park, Y.J., Marcogliese, P.C., Rosenfeld, J.A., Burrage, L.C., Liu, P., Murdock, D.R., Yamamoto, S., et al. (2020). De Novo Variants in CDK19 Are Associated with a Syndrome Involving Intellectual Disability and Epileptic Encephalopathy. Am J Hum Genet *106*, 717-725. 10.1016/j.ajhg.2020.04.001.
57. Bischof, J., Bjorklund, M., Furger, E., Schertel, C., Taipale, J., and Basler, K. (2013). A versatile platform for creating a comprehensive UAS-ORFeome library in Drosophila. Development *140*, 2434-2442. 10.1242/dev.088757.
58. Venken, K.J., He, Y., Hoskins, R.A., and Bellen, H.J. (2006). P[acman]: a BAC transgenic platform for targeted insertion of large DNA fragments in D. melanogaster. Science *314*, 1747-1751. 10.1126/science.1134426.
59. Kanca, O., Zirin, J., Hu, Y., Tepe, B., Dutta, D., Lin, W.W., Ma, L., Ge, M., Zuo, Z., Liu, L.P., et al. (2022). An expanded toolkit for Drosophila gene tagging using synthesized homology donor constructs for CRISPR-mediated homologous recombination. Elife *11*. 10.7554/eLife.76077.
60. Marcogliese, P.C., Dutta, D., Ray, S.S., Dang, N.D.P., Zuo, Z., Wang, Y., Lu, D., Fazal, F., Ravenscroft, T.A., Chung, H., et al. (2022). Loss of IRF2BPL impairs neuronal maintenance through excess Wnt signaling. Sci Adv *8*, eabl5613. 10.1126/sciadv.abl5613.
61. Nolo, R., Abbott, L.A., and Bellen, H.J. (2000). Senseless, a Zn finger transcription factor, is necessary and sufficient for sensory organ development in Drosophila. Cell *102*, 349-362. 10.1016/s0092-8674(00)00040-4.
62. Rentzsch, P., Schubach, M., Shendure, J., and Kircher, M. (2021). CADD-Splice-improving genome-wide variant effect prediction using deep learning-derived splice scores. Genome Med *13*, 31. 10.1186/s13073-021-00835-9.
63. Ioannidis, N.M., Rothstein, J.H., Pejaver, V., Middha, S., McDonnell, S.K., Baheti, S., Musolf, A., Li, Q., Holzinger, E., Karyadi, D., et al. (2016). REVEL: An Ensemble Method for Predicting the Pathogenicity of Rare Missense Variants. Am J Hum Genet *99*, 877-885. 10.1016/j.ajhg.2016.08.016.
64. Cheng, J., Novati, G., Pan, J., Bycroft, C., Zemgulyte, A., Applebaum, T., Pritzel, A., Wong, L.H., Zielinski, M., Sargeant, T., et al. (2023). Accurate proteome-wide missense variant effect prediction with AlphaMissense. Science *381*, eadg7492. 10.1126/science.adg7492.
65. Morrone, S., Cheng, Z., Moon, R.T., Cong, F., and Xu, W. (2012). Crystal structure of a Tankyrase-Axin complex and its implications for Axin turnover and Tankyrase substrate recruitment. Proc Natl Acad Sci U S A *109*, 1500-1505. 10.1073/pnas.1116618109.
66. Sondka, Z., Dhir, N.B., Carvalho-Silva, D., Jupe, S., Madhumita, McLaren, K., Starkey, M., Ward, S., Wilding, J., Ahmed, M., et al. (2024). COSMIC: a curated database of somatic variants and clinical data for cancer. Nucleic Acids Res *52*, D1210-D1217. 10.1093/nar/gkad986.
67. Evans, R., O'Neill, M., Pritzel, A., Antropova, N., Senior, A., Green, T., Žídek, A., Bates, R., Blackwell, S., Yim, J., et al. (2022). Protein complex prediction with AlphaFold-Multimer. bioRxiv, 2021.2010.2004.463034. 10.1101/2021.10.04.463034.
68. Abramson, J., Adler, J., Dunger, J., Evans, R., Green, T., Pritzel, A., Ronneberger, O., Willmore, L., Ballard, A.J., Bambrick, J., et al. (2024). Accurate structure prediction of

biomolecular interactions with AlphaFold 3. Nature *630*, 493-500. 10.1038/s41586-024-07487-w.

69. Guettler, S., LaRose, J., Petsalaki, E., Gish, G., Scotter, A., Pawson, T., Rottapel, R., and Sicheri, F. (2011). Structural Basis and Sequence Rules for Substrate Recognition by Tankyrase Explain the Basis for Cherubism Disease. Cell *147*, 1340-1354. 10.1016/j.cell.2011.10.046.

70. Teboul, L., Murray, S.A., and Nolan, P.M. (2017). Phenotyping first-generation genome editing mutants: a new standard? Mamm Genome *28*, 377-382. 10.1007/s00335-017-9711-x.

71. Liu, Y., Li, X., He, S., Huang, S., Li, C., Chen, Y., Liu, Z., Huang, X., and Wang, X. (2020). Efficient generation of mouse models with the prime editing system. Cell Discov *6*, 27. 10.1038/s41421-020-0165-z.

72. Adikusuma, F., Lushington, C., Arudkumar, J., Godahewa, G.I., Chey, Y.C.J., Gierus, L., Piltz, S., Geiger, A., Jain, Y., Reti, D., et al. (2021). Optimized nickase- and nuclease-based prime editing in human and mouse cells. Nucleic Acids Res *49*, 10785-10795. 10.1093/nar/gkab792.

73. Park, S.J., Jeong, T.Y., Shin, S.K., Yoon, D.E., Lim, S.Y., Kim, S.P., Choi, J., Lee, H., Hong, J.I., Ahn, J., et al. (2021). Targeted mutagenesis in mouse cells and embryos using an enhanced prime editor. Genome Biol *22*, 170. 10.1186/s13059-021-02389-w.

74. Gao, P., Lyu, Q., Ghanam, A.R., Lazzarotto, C.R., Newby, G.A., Zhang, W., Choi, M., Slivano, O.J., Holden, K., Walker, J.A., 2nd, et al. (2021). Prime editing in mice reveals the essentiality of a single base in driving tissue-specific gene expression. Genome Biol *22*, 83. 10.1186/s13059-021-02304-3.

75. Her, Y., Pascual, D.M., Goldstone-Joubert, Z., and Marcogliese, P.C. (2024). Variant functional assessment in Drosophila by overexpression: what can we learn? Genome *67*, 158-167. 10.1139/gen-2023-0135.

76. Swarup, S., and Verheyen, E.M. (2012). Wnt/Wingless signaling in Drosophila. Cold Spring Harb Perspect Biol *4*. 10.1101/cshperspect.a007930.

77. Nagarkar-Jaiswal, S., Lee, P.-T., Campbell, M.E., Chen, K., Anguiano-Zarate, S., Cantu Gutierrez, M., Busby, T., Lin, W.-W., He, Y., Schulze, K.L., et al. (2015). A library of MiMICs allows tagging of genes and reversible, spatial and temporal knockdown of proteins in Drosophila. eLife *4*, e05338. 10.7554/eLife.05338.

78. Roht, L., Hyldebrandt, H.K., Stormorken, A.T., Nordgarden, H., Sijmons, R.H., Bos, D.K., Riegert-Johnson, D., Mantia-Macklin, S., Ilves, P., Muru, K., et al. (2023). AXIN2-related oligodontia-colorectal cancer syndrome with cleft palate as a possible new feature. Molecular Genetics & Genomic Medicine *11*, e2157. https://doi.org/10.1002/mgg3.2157.

79. Macklin- Mantia, S.K., Hines, S.L., Chaichana, K.L., Donaldson, A.M., Ko, S.L., Zhai, Q., Samadder, N.J., and Riegert-Johnson, D.L. (2020). Case report expanding the germline AXIN2- related phenotype to include olfactory neuroblastoma and gastric adenoma. BMC Medical Genetics *21*, 161. 10.1186/s12881-020-01103-0.

80. Yu, H.-M.I., Jerchow, B., Sheu, T.-J., Liu, B., Costantini, F., Puzas, J.E., Birchmeier, W., and Hsu, W. (2005). The role of Axin2 in calvarial morphogenesis and craniosynostosis. Development *132*, 1995-2005. 10.1242/dev.01786.

81. Yan, Y., Tang, D., Chen, M., Huang, J., Xie, R., Jonason, J.H., Tan, X., Hou, W., Reynolds, D., Hsu, W., et al. (2009). Axin2 controls bone remodeling through the β-catenin–BMP signaling pathway in adult mice. Journal of Cell Science *122*, 3566-3578. 10.1242/jcs.051904.

82. de Roo, J.J.D., Breukel, C., Chhatta, A.R., Linssen, M.M., Vloemans, S.A., Salvatori, D., Mikkers, H.M.M., Verbeek, S.J., and Staal, F.J.T. (2017). Axin2-mTurquoise2: A novel reporter mouse model for the detection of canonical Wnt signalling. genesis *55*, e23068. https://doi.org/10.1002/dvg.23068.

83. Mazzoni, S.M., Petty, E.M., Stoffel, E.M., and Fearon, E.R. (2015). An AXIN2 Mutant Allele Associated With Predisposition to Colorectal Neoplasia Has Context-Dependent Effects on AXIN2 Protein Function. Neoplasia *17*, 463-472. https://doi.org/10.1016/j.neo.2015.04.006.
84. Janeckova, E., Feng, J., Guo, T., Han, X., Ghobadi, A., Araujo-Villalba, A., Rahman, M.S., Ziaei, H., Ho, T.V., Pareek, S., et al. (2023). Canonical Wnt signaling regulates soft palate development by mediating ciliary homeostasis. Development *150*. 10.1242/dev.201189.
85. Iwata, J., Suzuki, A., Yokota, T., Ho, T.V., Pelikan, R., Urata, M., Sanchez-Lara, P.A., and Chai, Y. (2014). TGFbeta regulates epithelial-mesenchymal interactions through WNT signaling activity to control muscle development in the soft palate. Development *141*, 909-917. 10.1242/dev.103093.
86. Maupin, K.A., Droscha, C.J., and Williams, B.O. (2013). A Comprehensive Overview of Skeletal Phenotypes Associated with Alterations in Wnt/beta-catenin Signaling in Humans and Mice. Bone Res *1*, 27-71. 10.4248/BR201301004.
87. Micchelli, C.A., Rulifson, E.J., and Blair, S.S. (1997). The function and regulation of cut expression on the wing margin of Drosophila: Notch, Wingless and a dominant negative role for Delta and Serrate. Development *124*, 1485-1495. 10.1242/dev.124.8.1485.
88. Legent, K., and Treisman, J.E. (2008). Wingless signaling in Drosophila eye development. Methods Mol Biol *469*, 141-161. 10.1007/978-1-60327-469-2_12.

A

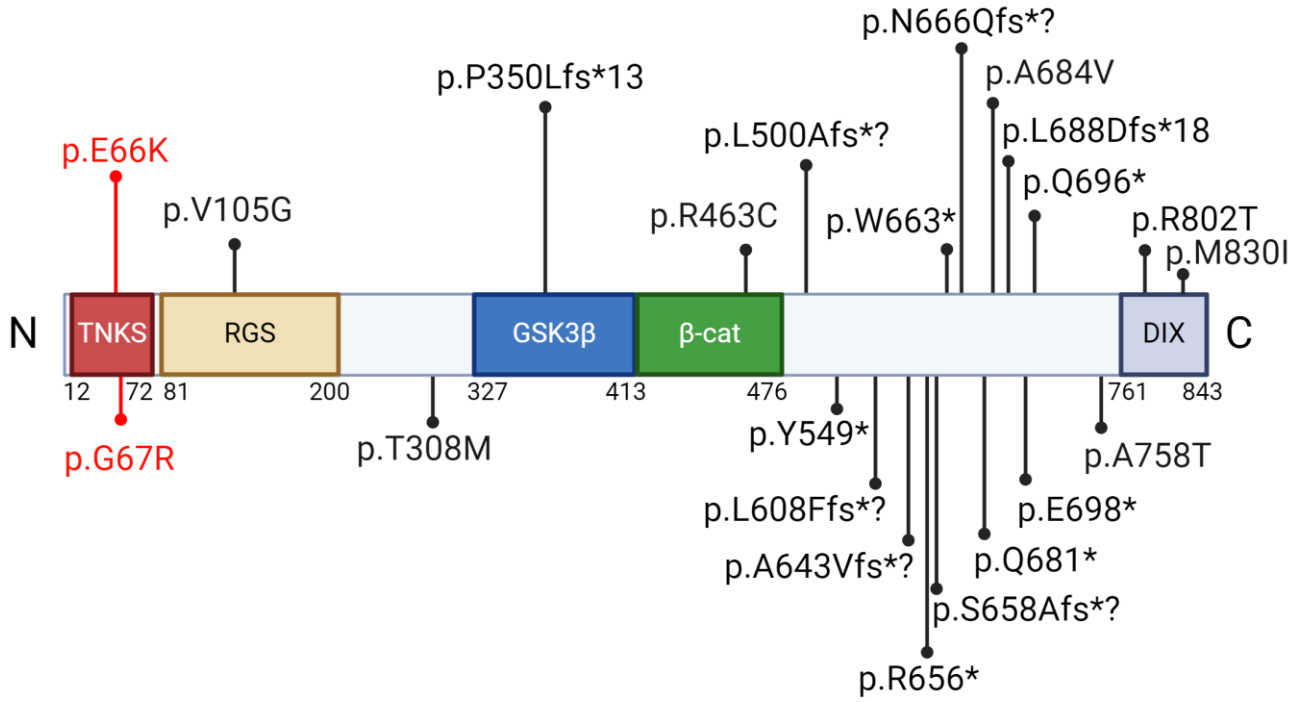
p.N666Qfs*?
p.A684V
p.P350Lfs*13
p.L688Dfs*18
p.L500Afs*?
p.E66K
p.Q696*
p.V105G
p.R463C
p.W663*
p.R802T
p.M830I
N
TNKS
RGS
GSK3β
β-cat
DIX
C
12
72
81
200
327
413
476
761
843
p.Y549*
p.G67R
p.T308M
p.A758T
p.L608Ffs*?
p.E698*
p.A643Vfs*?
p.Q681*
p.S658Afs*?
p.R656*

B

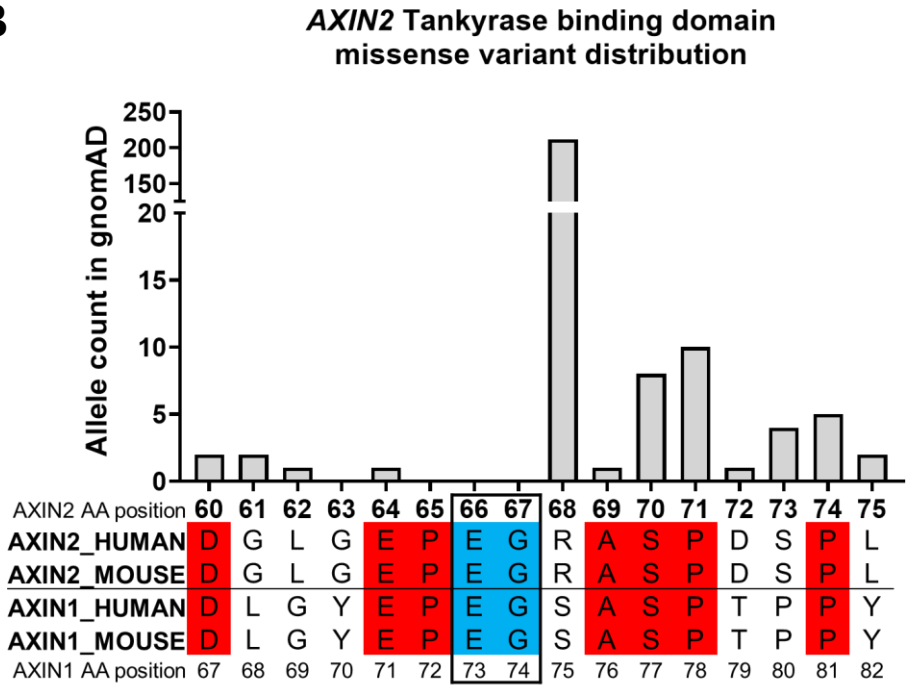
AXIN2 Tankyrase binding domain missense variant distribution
Allele count in gnomAD
250
200
150
20
15
10
5
0
AXIN2 AA position 60 61 62 63 64 65 66 67 68 69 70 71 72 73 74 75
AXIN2_HUMAN D G L G E P E G R A S P D S P L
AXIN2_MOUSE D G L G E P E G R A S P D S P L
AXIN1_HUMAN D L G Y E P E G S A S P T P P Y
AXIN1_MOUSE D L G Y E P E G S A S P T P P Y
AXIN1 AA position 67 68 69 70 71 72 73 74 75 76 77 78 79 80 81 82

Figure 1.

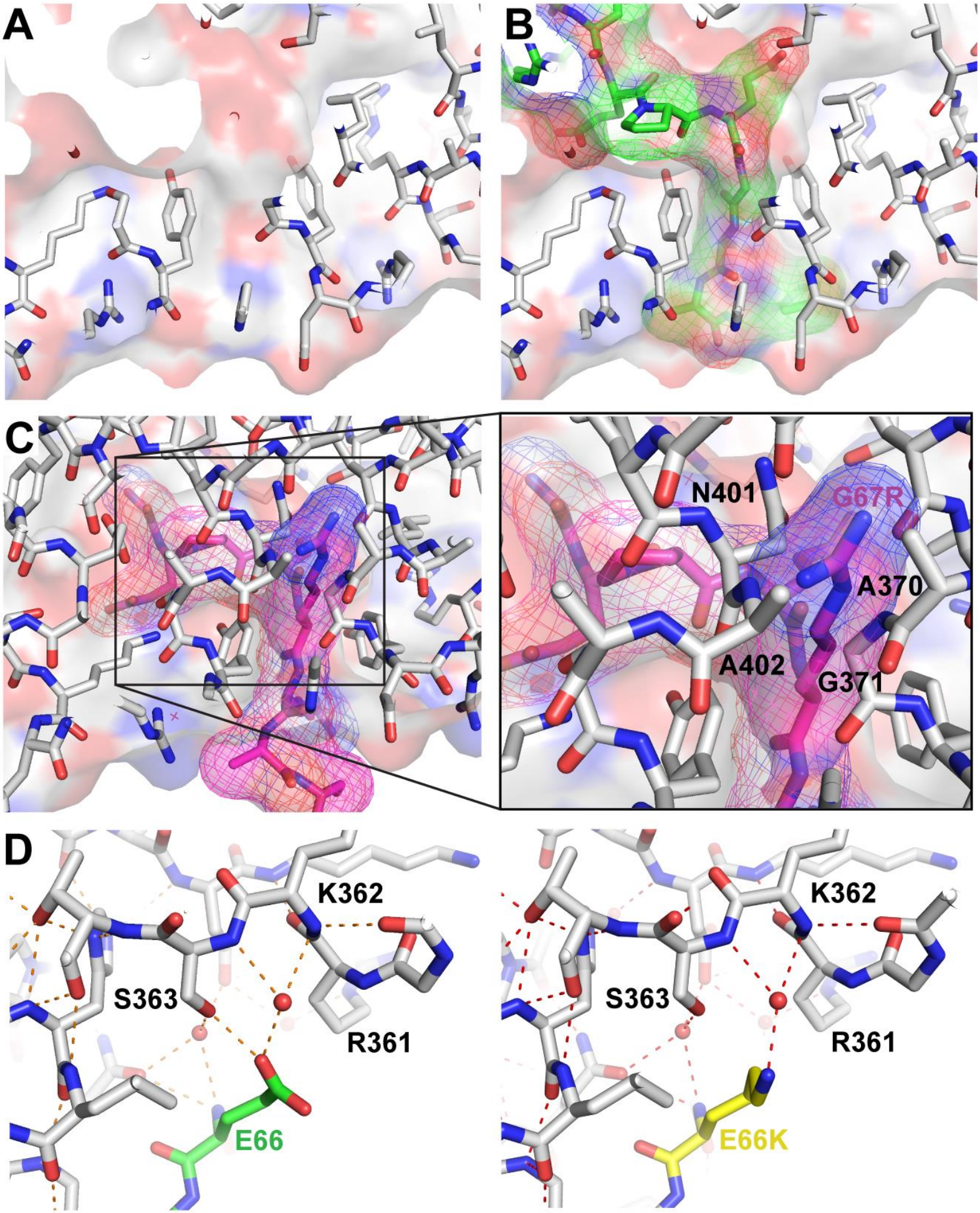
A
B
C
N401
G67R
A370
A402
G371
D
K362
S363
R361
E66
K362
S363
R361
E66K

Figure 2.

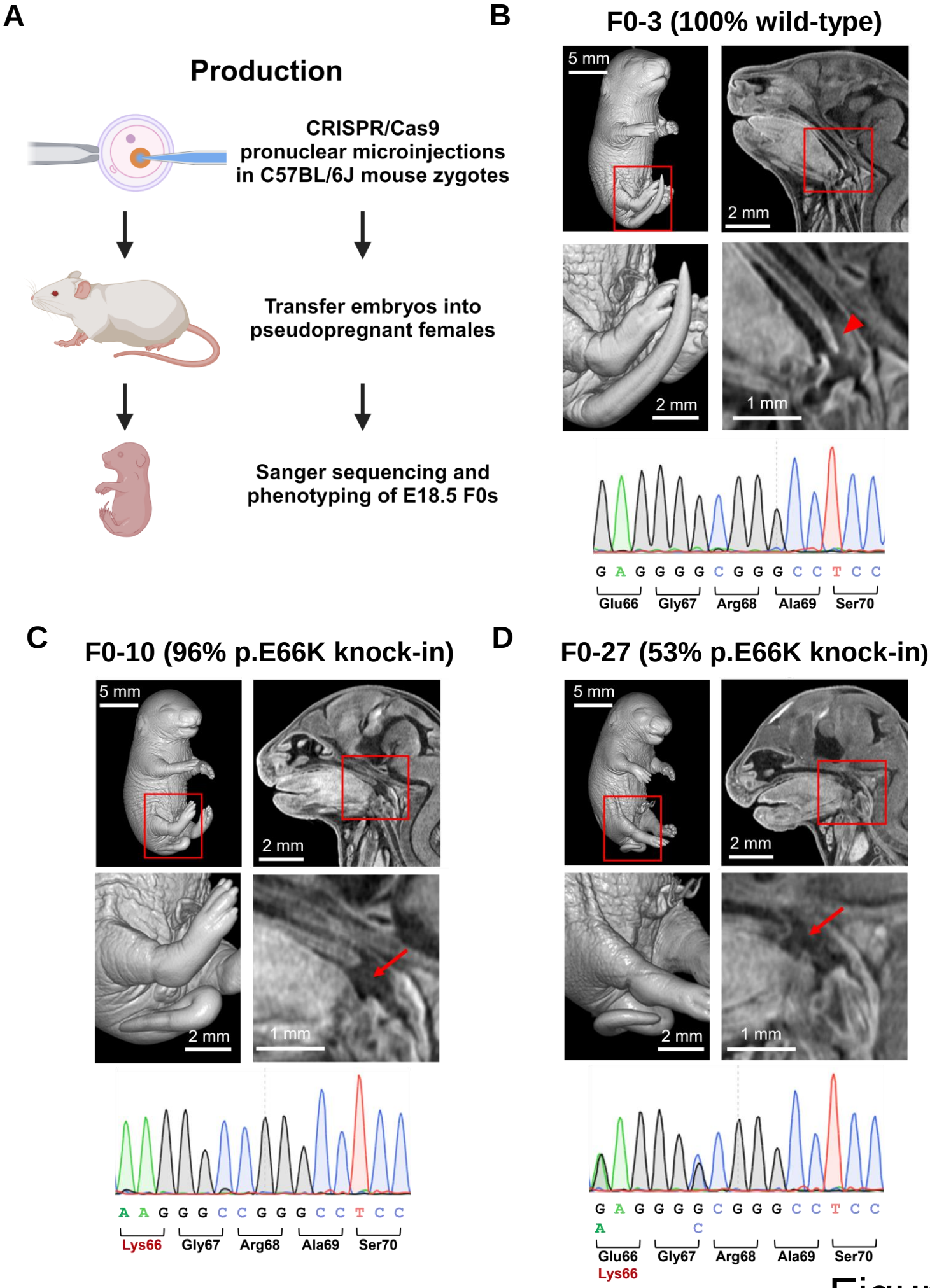
A
Production
CRISPR/Cas9
pronuclear microinjections
in C57BL/6J mouse zygotes
Transfer embryos into
pseudopregnant females
Sanger sequencing and
phenotyping of E18.5 F0s
B
F0-3 (100% wild-type)
5 mm
2 mm
2 mm
1 mm
G A G G G G C G G G C C T C C
Glu66 Gly67 Arg68 Ala69 Ser70
C
F0-10 (96% p.E66K knock-in)
5 mm
2 mm
2 mm
1 mm
A A G G G C C G G G C C T C C
Lys66 Gly67 Arg68 Ala69 Ser70
D
F0-27 (53% p.E66K knock-in)
5 mm
2 mm
2 mm
1 mm
G A G G G G C G G G C C T C C
A C
Glu66 Gly67 Arg68 Ala69 Ser70
Lys66

Figure 3.

A

Production

Prime editing (PE) → F0s genotyped and Sanger sequenced → Mosaic male founder identified

N1 Screen

Axin2 p.E66K PE founder × C57BL/6J females → Live birth genotyping and phenotyping

Axin2 p.E66K PE founder → IVF C57BL/6J oocytes → E18.5 genotyping and phenotyping

B

Genotype	Timepoint		p-value
	E18.5 (n)	Postnatal (n)	
Axin2$^{+/+}$	15	30	<0.0001
Axin2$^{E66K/+}$	14	0	

C

N1-6 (*Axin2*$^{+/+}$)

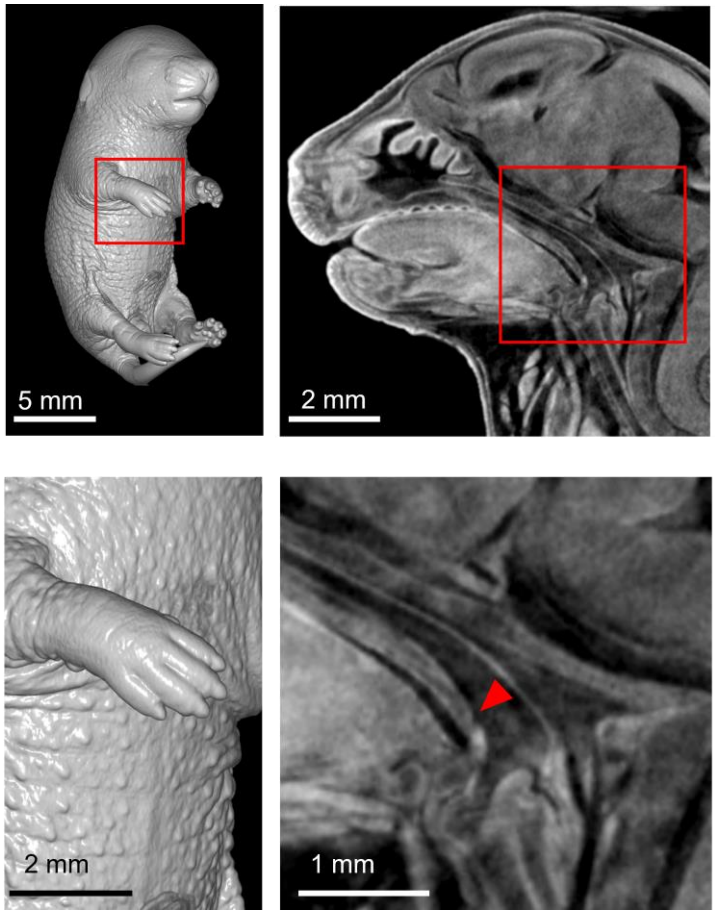

D

N1-19 (*Axin2*$^{E66K/+}$)

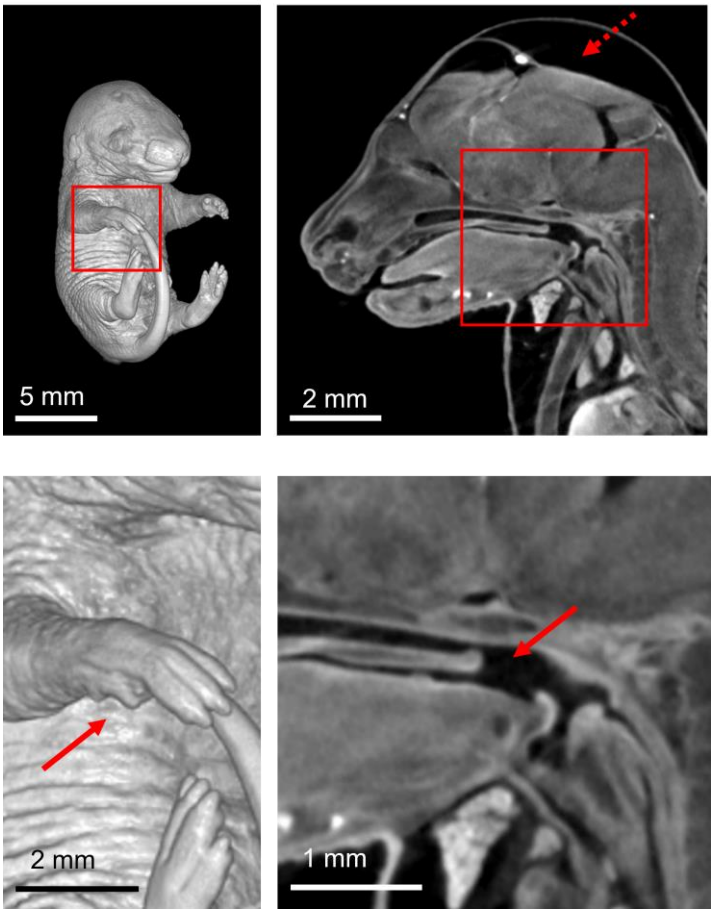

Figure 4.

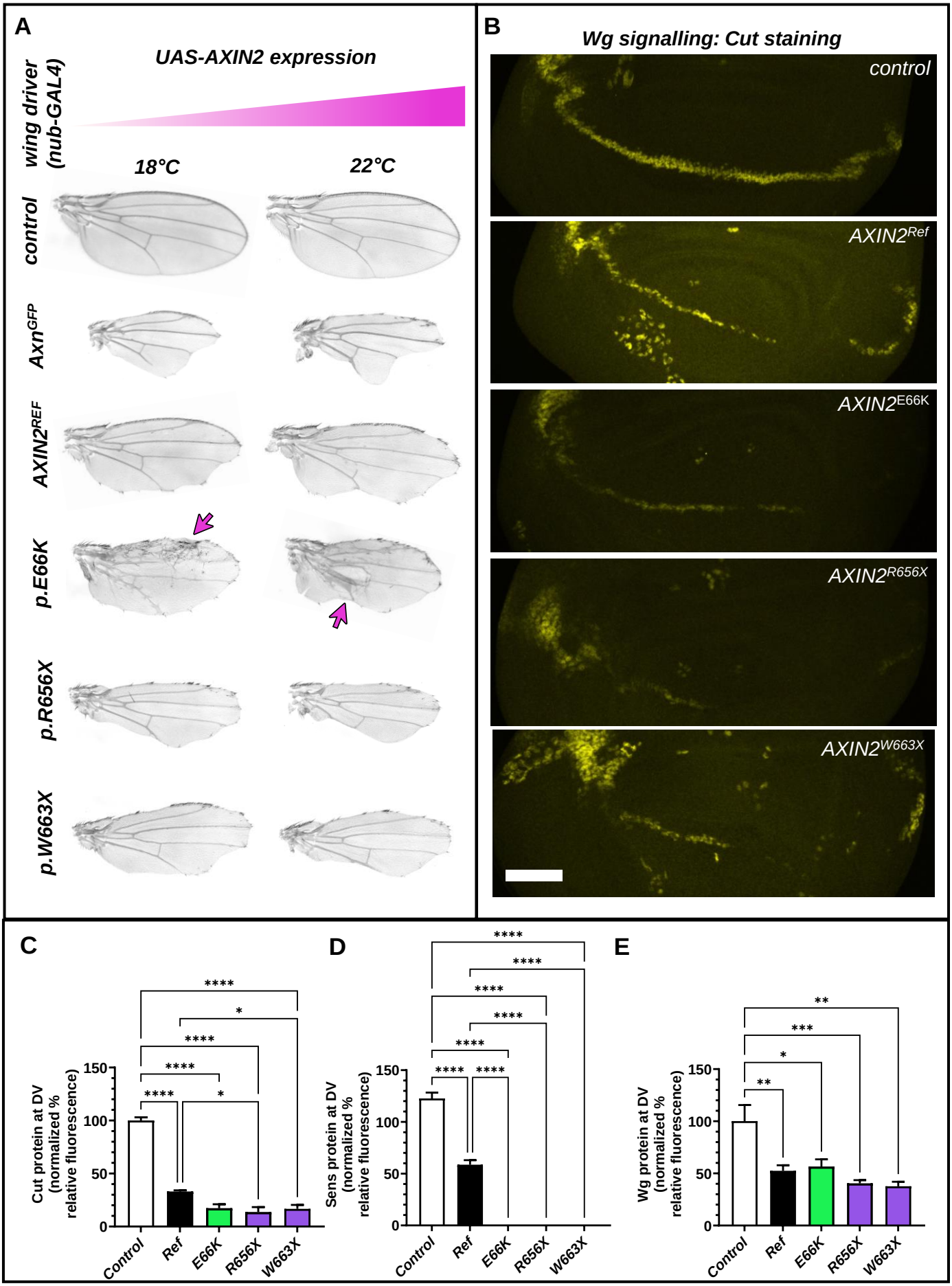
A
UAS-AXIN2 expression
wing driver (nub-GAL4)
18°C
22°C
control
Axn^GFP
AXIN2^REF
p.E66K
p.R656X
p.W663X
B
Wg signalling: Cut staining
control
AXIN2^Ref
AXIN2^E66K
AXIN2^R656X
AXIN2^W663X
C
Cut protein at DV (normalized % relative fluorescence)
D
Sens protein at DV (normalized % relative fluorescence)
E
Wg protein at DV (normalized % relative fluorescence)
Control
Ref
E66K
R656X
W663X

Figure 5.

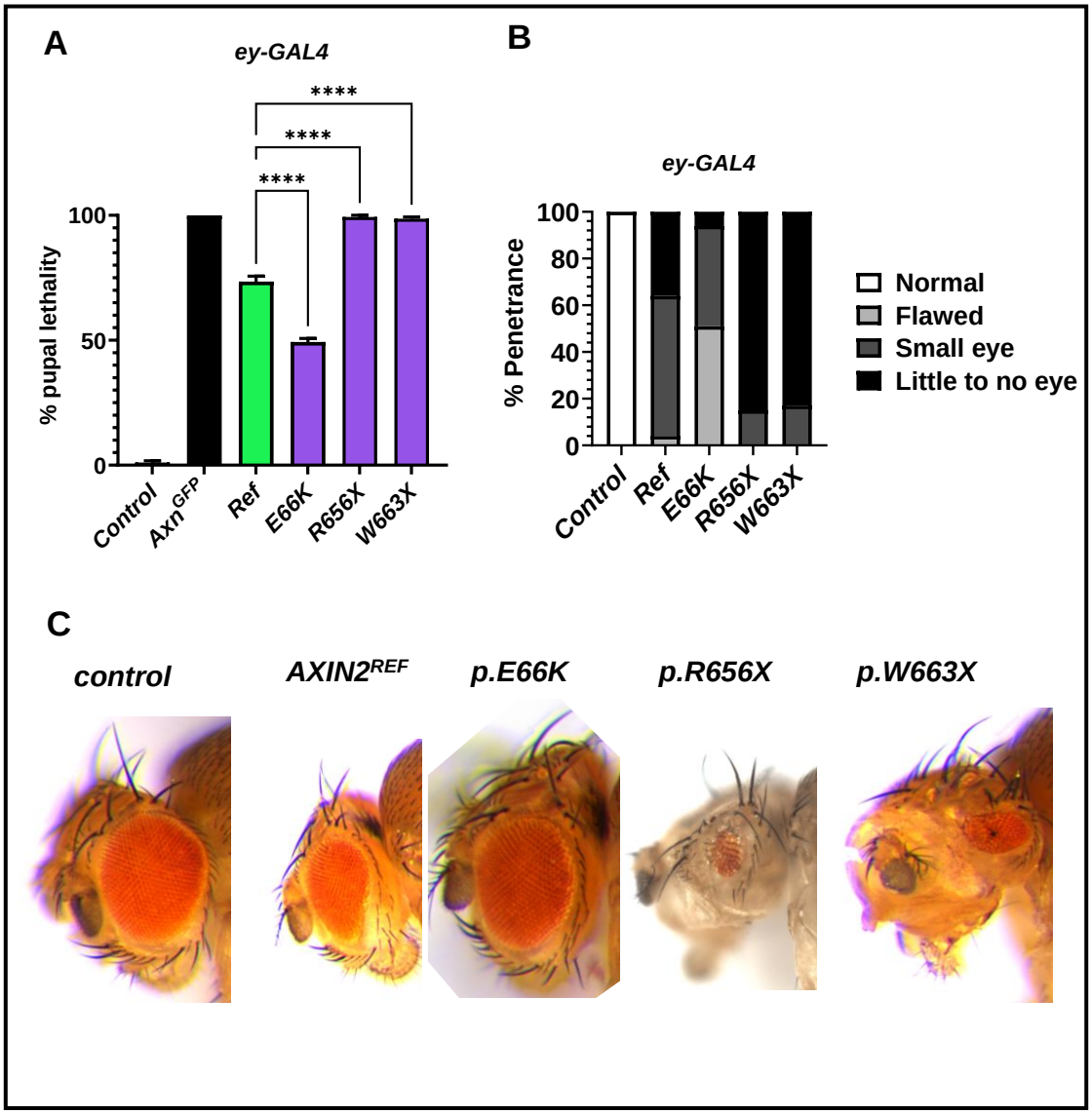
A
ey-GAL4
****
****
****
100
50
0
% pupal lethality
Control
Axn GFP
Ref
E66K
R656X
W663X
B
ey-GAL4
100
80
60
40
20
0
% Penetrance
Control
Ref
E66K
R656X
W663X
Normal
Flawed
Small eye
Little to no eye
C
control
AXIN2REF
p.E66K
p.R656X
p.W663X

Figure 6.